### nature microbiology

**Article** 

https://doi.org/10.1038/s41564-025-02027-2

# Cyclic-di-AMP modulates cellular turgor in response to defects in bacterial cell wall synthesis

Received: 19 September 2024

Anna P. Brogan¹, Paola Bardetti², Enrique R. Rojas **®** <sup>2</sup> & David Z. Rudner **®** <sup>1</sup> ⊠

Accepted: 1 May 2025

Published online: 17 June 2025



Cyclic-di-AMP (c-di-AMP) is an essential second messenger in *Bacillus subtilis* and many other Gram-positive bacteria. Work over the past decade has revealed that this cyclic nucleotide controls cation and osmolyte transporters, leading to the hypothesis that c-di-AMP regulates cytoplasmic turgor pressure. Although the targets of c-di-AMP are well established, the signals that control the levels of this second messenger and the factors that transduce these signals are unknown. Here we report that c-di-AMP levels are modulated by the cyclase regulator CdaR in response to cell wall defects. We further demonstrate that changing the levels of c-di-AMP alters turgor pressure. Our data support a model in which CdaR senses defects in the cell wall and activates c-di-AMP synthesis in response. The increase in c-di-AMP reduces turgor, preventing lysis and enabling fortification of the peptidoglycan meshwork. Thus, a central function of c-di-AMP is to control cellular turgor in response to envelope defects.

Nearly all organisms use nucleotide analogues as second messengers in response to changing environmental and physiological conditions. Cyclic-di-AMP (c-di-AMP) is a broadly conserved signalling molecule that is essential for viability in many Gram-positive bacteria, including the human pathogens Staphylococcus aureus, Listeria monocytogenes and Clostridioides difficile<sup>1-5</sup>. Work over the past decade has revealed that c-di-AMP's principal and essential function is to control the expression and activity of osmolyte transporters<sup>6</sup>. Insights from Bacillus subtilis provide a framework to understand this activity: in B. subtilis, c-di-AMP binds to and inhibits K<sup>+</sup> and compatible solute importers, and activates K<sup>+</sup> exporters<sup>7-10</sup>. In addition, riboswitches that bind c-di-AMP inhibit transcription of K<sup>+</sup> importer genes<sup>11,12</sup>. Accordingly, high levels of the second messenger reduce intracellular osmolyte concentration, while low c-di-AMP levels increase intracellular osmolarity. These findings have led to the hypothesis that c-di-AMP controls cytoplasmic turgor pressure<sup>13,14</sup>. In the context of this model, low c-di-AMP levels increase turgor pressure, while high c-di-AMP levels decrease it.

This hypothesis provides an explanation for the well documented link between c-di-AMP and antibiotics that target cell wall synthesis<sup>14</sup>. The cell wall that surrounds bacteria provides structural integrity

and prevents lysis due to high cytoplasmic turgor pressure. This rigid meshwork, known as peptidoglycan (PG), is made of glycan strands crosslinked together by short peptides and is essential for viability in nearly all bacteria<sup>15</sup>. In rod-shaped bacteria such as B. subtilis, the PG meshwork is built by two types of cell wall synthases: the class A penicillin-binding proteins (aPBPs) and complexes of a SEDS (shape, elongation, division, sporulation) protein with its cognate class B PBP (bPBP)<sup>15</sup>. SEDS-bPBP cell wall synthesis occurs within a larger membrane complex (called the elongasome) that is guided by filament-forming proteins in the cytoplasm. The elongasome is essential for cell elongation and generates glycan strands that are oriented perpendicular to the long axis of the cell. The aPBP enzymes are thought to fortify these glycan strands by synthesizing peptidoglycan between them<sup>16</sup>. Both synthases are required to generate a robust cell wall, but how cells monitor the assembly of this essential matrix to prevent aberrant lysis remains poorly understood.

In *B. subtilis, S. aureus, Streptococcus pneumoniae* and other Gram-positive pathogens, mutations that increase c-di-AMP levels confer resistance to  $\beta$ -lactams and other cell wall targeting antibiotics <sup>17-20</sup>. Reciprocally, mutations that reduce levels of the signalling nucleotide

<sup>1</sup>Department of Microbiology, Harvard Medical School, Boston, MA, USA. <sup>2</sup>Department of Biology, New York University, New York, NY, USA. ⊠e-mail: rudner@hms.harvard.edu

increase susceptibility to these drugs  $^{5,17,21-25}$ . In these bacteria, c-di-AMP does not appear to target cell wall biogenesis factors. Thus, the changes in antibiotic resistance have been proposed to result from changes in turgor pressure  $^{13,14}$ . Mutants with high c-di-AMP that are predicted to reduce turgor pressure resist  $\beta$ -lactam killing. Reciprocally, mutants with low c-di-AMP are more prone to lysis in the presence of these drugs due to high turgor. While this model is compelling in its simplicity, direct evidence that c-di-AMP levels impact turgor is lacking.

Bacteria often encode several enzymes that synthesize and degrade c-di-AMP. Diadenylate cyclase (DAC) domains synthesize the cyclic nucleotide through condensation of two ATP molecules. Phosphodiesterases linearize the cyclic substrate to pApA and transporters export c-di-AMP. Many of these enzymes and their putative regulators are conserved among c-di-AMP-containing bacteria<sup>6</sup>. B. subtilis encodes three DACs: CdaA, DisA and the sporulation-specific CdaS. It also contains two phosphodiesterases, GdpP and PgpH. Although the activities of these broadly conserved enzymes have been well established, the regulatory mechanisms that control their functions remain elusive. Nearly all bacteria that produce c-di-AMP contain the cyclase CdaA (also known as DacA in some species) and its putative regulator CdaR<sup>26</sup>. CdaR has a single transmembrane (TM) segment that interacts with the membrane domain of CdaA, followed by repeated YbbR domains of unknown function<sup>3,22</sup>. In a subset of bacteria, including B. subtilis, a long intrinsically disordered region (IDR) with little sequence-level conservation follows the YbbR repeats. The signal(s) that CdaR responds to remains unknown.

Here we extend previous studies by showing that low c-di-AMP levels increase susceptibility to genetic and chemical perturbations to cell envelope biogenesis, while high c-di-AMP levels protect the cell from lysis. This analysis led us to discover that *B. subtilis* increases c-di-AMP levels in a CdaA-dependent manner in response to a reduction in aPBP cell wall synthesis. We show that CdaR's IDR is required to increase c-di-AMP and to maintain viability when PG biogenesis is perturbed. IDRs from CdaR homologues can function in place of the native IDR on the B. subtilis regulator, suggesting that its regulatory function is broadly conserved. Furthermore, IDRs from two other B. subtilis proteins implicated in monitoring the cell wall can also replace CdaR's IDR. Finally, we demonstrate that increasing c-di-AMP levels reduces cytoplasmic turgor pressure, and that decreasing the second messenger increases turgor. Collectively, our data define a signalling pathway in which CdaR's IDR senses cell envelope defects and activates CdaA in response. The increase in c-di-AMP reduces turgor and protects the cell from lysis.

#### Results

#### c-di-AMP is critical in the presence of cell envelope defects

Previous studies have found that mutations in c-di-AMP-degrading enzymes provide resistance to β-lactam antibiotics<sup>17-20</sup>. To more directly investigate the relationship between c-di-AMP and cell wall synthesis in B. subtilis, we used an IPTG-regulated allele of pbp1 (also known as ponA) encoding the major aPBP cell wall synthase, PBP1. Depletion of this enzyme causes impaired growth, cell wall defects and lysis<sup>27</sup>. We introduced loss-of-function mutations in each of the c-di-AMP cyclases into the P<sub>IPTG</sub>-pbp1 strain and analysed growth. As can be seen in Fig. 1a, depletion of PBP1 in cells lacking disA or cdaS resembled the parental strain. However, growth was modestly impaired in cells lacking cdaA and the cdaAR operon upon PBP1 depletion (Fig. 1a). The growth defect was more pronounced in a pbp1 null mutant (Supplementary Fig. 1a,b). Furthermore, a stably expressed CdaA catalytic mutant (D171A) phenocopied the *cdaA* null, consistent with the requirement for cyclase activity (Fig. 1a,b and Supplementary Fig. 1a,b)<sup>28</sup>. Fluorescence imaging revealed that the  $\Delta pbp1$  cdaA mutants had aberrant morphologies and envelope integrity defects, as assayed by propidium iodide (PI) (Fig. 1c,d). Thus, c-di-AMP synthesis by CdaA is important for envelope integrity and growth when cell wall synthesis is impaired.

To investigate whether increased levels of c-di-AMP can suppress severe cell wall defects, we took advantage of the synthetic relationship between pbp1 and gpsB, which encodes a scaffold protein for enzymes involved in PG biogenesis<sup>29</sup>. Neither gene is essential but cells depleted of PBP1 in the absence of gpsB have severe cell wall defects and are strongly impaired in growth (Fig. 1e)<sup>30</sup>. We found that deletion of cdaA or cdaAR in this background caused cell death, consistent with the synthetic growth defect of the  $\Delta pbp1 \Delta cdaA$  mutant. Conversely, cells lacking the phosphodiesterases, GdpP or PgpH, that increase c-di-AMP levels restored some viability to the  $\Delta gpsB$  mutant depleted of PBP1 (Fig. 1e). We conclude that reducing c-di-AMP levels is toxic, while increasing c-di-AMP levels is suppressive in this cell wall defective mutant.

Next, we systematically analysed the relationship between c-di-AMP levels and cell envelope-targeting antibiotics. To do so, we deleted the native copies of all three c-di-AMP synthases (\$\( \textit{\textit{D}}\) das \$\textit{\textit{A}}\) das \$\textit{A}\) and strain harbouring an IPTG-regulated allele of \$cdaA\$ at an ectopic chromosomal locus. Expression of \$CdaA\$ at low levels (5–10 \( \text{µM} \)) led to a reduction in growth in the presence of all antibiotics tested, consistent with previous observations in other bacteria (Fig. 1f and Extended Data Fig. 1a) \$1,721,22,24,25\$. Reciprocally, overexpression of \$cdaA\$, combined with deletions of the two genes encoding c-di-AMP phosphodiesterases improved growth (Fig. 1f and Extended Data Fig. 1b). Consistent with these findings, cells expressing low levels of \$CdaAR\$ as the sole cyclase were inviable in the absence of PBP1 (Supplementary Fig. 3). Thus, when the cell wall is compromised, high levels of c-di-AMP improve growth, while low levels of the second messenger impair viability.

#### c-di-AMP levels increase in response to loss of PBP1

The experiments described above led us to hypothesize that B. subtilis actively monitors its PG meshwork and, in response to defects, activates CdaA to increase c-di-AMP levels and reduce intracellular osmolarity. The predicted decrease in turgor pressure would protect the cell from lysis and possibly facilitate repair of the cell wall. To investigate this model, we built an in vivo reporter to monitor c-di-AMP levels using a c-di-AMP riboswitch. The 5' UTR of the B. subtilis kimA gene that encodes a K<sup>+</sup> importer folds into a transcriptional terminator when bound to c-di-AMP<sup>11</sup> (Fig. 2a). When c-di-AMP levels are high, transcription of kimA is reduced; when levels of the second messenger drop, there is less termination and increased expression (Fig. 2a). We inserted this riboswitch between the constitutive promoter  $P_{veg}$  and lacZ. Thus, the levels of  $\beta$ -galactosidase activity inversely correlate with the levels of c-di-AMP (Fig. 2a). We validated the reporter using our strain lacking the native cyclases and harbouring an IPTG-regulated allele of cdaAR. Low CdaAR expression results in low c-di-AMP levels and high β-galactosidase activity. Increasing CdaAR expression increases c-di-AMP and decreases reporter activity (Fig. 2b,c). The ranges in β-galactosidase activity and c-di-AMP levels in this strain were 2.4- and 1.4-fold, respectively. The experiments presented in Fig. 1f and Extended Data Fig. 1 indicate that these relatively modest changes are physiologically relevant. Similarly, a strain lacking *cdaAR* had a 1.3-fold increase in β-galactosidase activity, while the  $\Delta gdpP$  mutant had a 1.3-fold decrease (Extended Data Fig. 2a). Thus, B. subtilis modulates this second messenger over a narrow range.

We used our riboswitch reporter to monitor relative levels of c-di-AMP in the presence and absence of PBP1 in a strain in which the only cyclase was CdaA (with its regulator CdaR) expressed under IPTG control. As can be seen in Fig. 2d, cells lacking PBP1 had 1.7-fold less β-galactosidase activity than PBP1+ cells. Importantly, CdaA protein levels remained unchanged in the PBP1 mutant (Fig. 2e). A similar reduction in reporter activity (1.7-fold) was observed in cells treated with moenomycin that inhibits the glycosyltransferase activity of class A PBPs, including PBP1 (ref. 31) (Fig. 2d). Thus, *B. subtilis* cells lacking aPBP activity increase the production of c-di-AMP. Interestingly, this response was specific to moenomycin, as c-di-AMP levels were unaffected by other cell envelope-targeting drugs (Extended

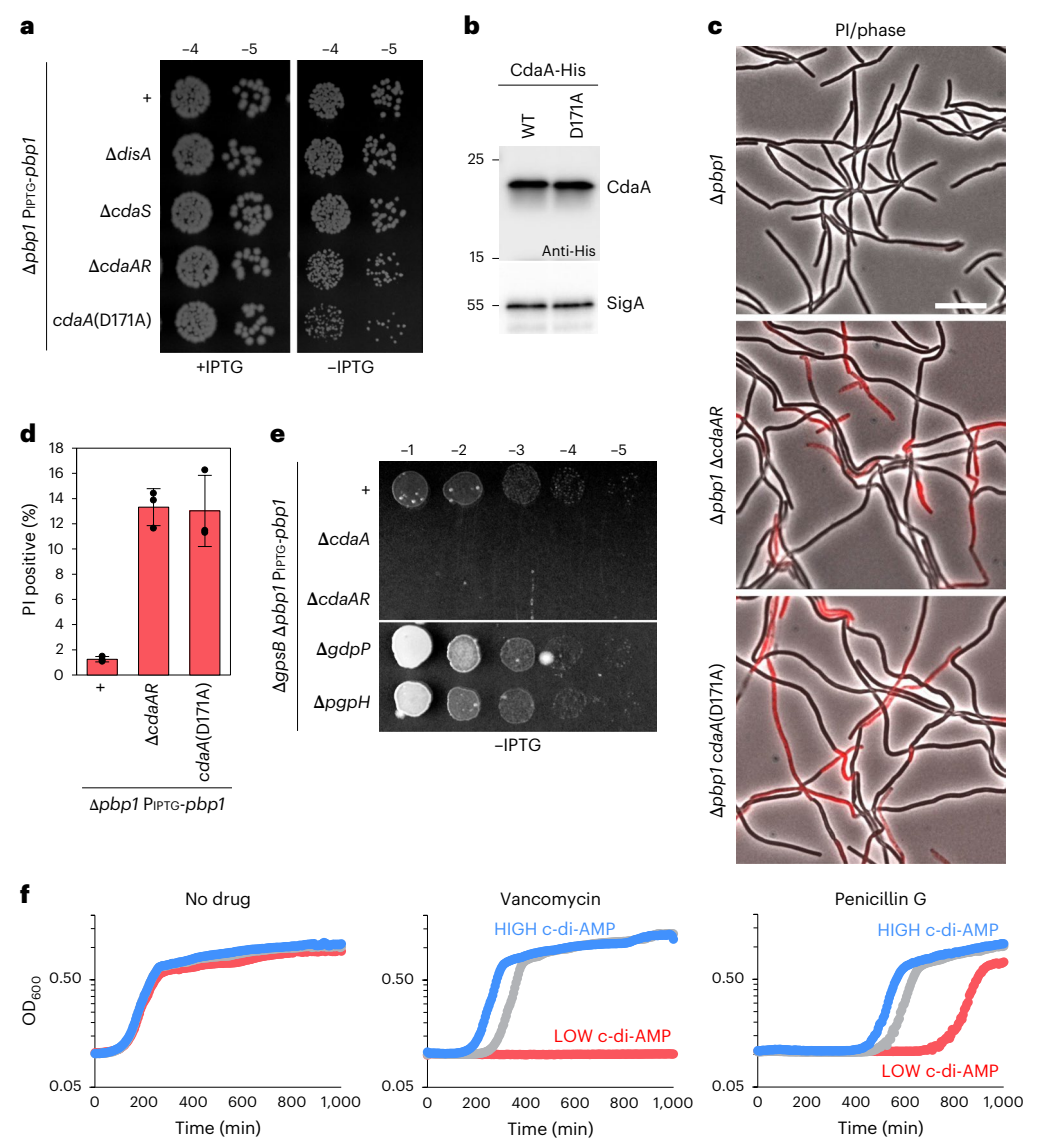


**Fig. 1** | **CdaA-dependent** c-**di-AMP** synthesis is important for cell envelope integrity. **a**, Serial dilutions (10-fold) of the indicated strains were spotted on LB agar in the presence or absence of 50 μM IPTG. All five strains express PBP1 under IPTG control. The catalytic mutation (D171A) is located at the native cdaA locus. **b**, Representative immunoblots of B. subtills cells with a functional CdaA-His fusion or the catalytic point mutant (D171A) (Supplementary Fig. 5a). Both are expressed under IPTG control at an ectopic locus in the presence of 50 μM IPTG. SigA controls for loading. Molecular weight markers in kDa are indicated. **c**, Representative merged phase-contrast and fluorescence images of the indicated exponentially growing B. subtilis strains stained with propidium iodide (PI). Scale bar, 5 μm. **d**, Quantification of PI-positive cells from images as

in **c**. Means  $\pm$  s.d. are shown; n (single cell) = 1,670, 1,347, 1,182 (WT), n = 1,019, 1,031, 1,178 ( $\Delta ponA \ \Delta cdaAR$ ), n = 1,106, 813, 994 ( $\Delta ponA \ cdaA$ -D171A). **e**, Serial dilutions (10-fold) of the indicated strains were spotted on LB agar in the absence of IPTG. The photograph is of a single agar plate with unrelated spots cropped out. **f**, Representative growth curves of  $\Delta disA \ \Delta cdaS \ \Delta cdaAR \ P_{IPTG}$ -cdaA grown with 10  $\mu$ M (red) or 50  $\mu$ M (grey) IPTG and  $\Delta disA \ \Delta cdaS \ \Delta cdaAR \ \Delta gdaP \ \Delta pgpH$   $P_{IPTG}$ -cdaA grown with 500  $\mu$ M (blue) IPTG in the presence of sub-inhibitory concentrations of the indicated antibiotics. IPTG at 50  $\mu$ M is closest to physiological expression levels (Extended Data Fig. 3e). All experiments in this figure were performed in biological triplicate and a representative experiment is shown.

Data Fig. 2b) (see Discussion). For simplicity, we refer to defects caused by loss of aPBP PG synthesis as cell wall defects, although the increase in c-di-AMP is specific to this type of defect. Importantly, a graded decrease in the levels of PBP1, using our IPTG-regulated allele, caused a graded increase in c-di-AMP (Fig. 2f). Thus, the magnitude of the response correlates with the extent of cell wall defects. Importantly, this response was specific to CdaAR, as c-di-AMP levels did not increase upon deletion of PBP1 when DisA was the sole cyclase (Extended Data Fig. 2c). Furthermore, the DisA-expressing cells had reduced viability compared with the CdaAR-expressing cells in the absence of PBP1 (Extended Data Fig. 2d), consistent with the idea that the CdaA-dependent increase in c-di-AMP is critical for survival when cell wall synthesis is compromised.

#### CdaR's IDR is required for viability during envelope stress

To investigate the molecular basis of CdaA activation in response to cell wall stress, we focused on its putative regulator CdaR. CdaR contains a single TM segment that interacts with the membrane domain of CdaA, followed by repeated YbbR domains of unknown function (Fig. 3a)<sup>3,22</sup>. Many CdaR family members, largely in the Bacilli, Enterococci and Clostridia phyla, have extracytoplasmic IDRs appended to their YbbR repeats (Fig. 3a and Supplementary Fig. 4). Unlike the rest of the CdaR protein, this region is poorly conserved, yet is composed of similar hydrophilic and charged amino acids (Fig. 3b). Recently, we showed that the extracytoplasmic IDRs on two other *B. subtilis* proteins, RsgI and PBP1, are involved in responding to cell envelope defects<sup>30</sup>. Intriguingly, these IDRs have little sequence-level conservation but

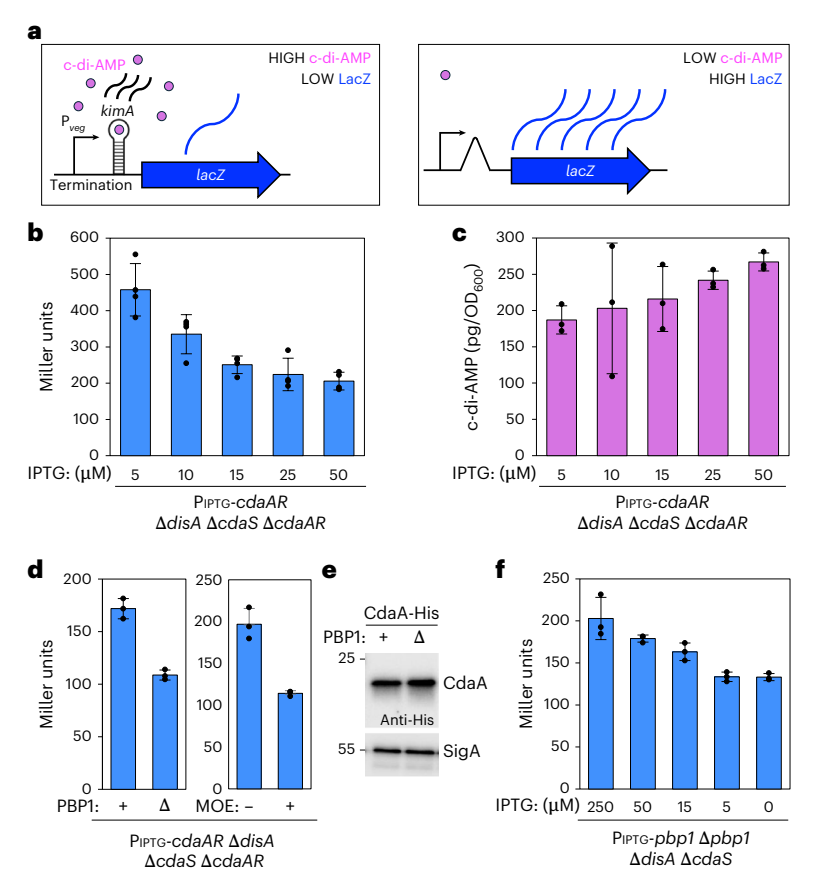


Fig. 2 | c-di-AMP levels increase in response to impaired cell wall synthesis. a, Schematic of the c-di-AMP-binding riboswitch reporter used to monitor c-di-AMP levels. Cyclic-di-AMP binds the *kimA* RNA hairpin, generating a transcriptional terminator upstream of *lacZ*. b, Bar graph showing β-galactosidase activity from the riboswitch reporter in the indicated *B. subtilis* strains lacking the native cyclases and harbouring an IPTG-regulated allele of *cdaAR*. Cells were grown in LB with the indicated IPTG concentrations for >5 generations before assaying. c, Bar graph showing c-di-AMP levels quantified by ELISA and normalized to  $OD_{600}$  in the same conditions as in b. d, Bar graph

showing  $\beta$ -galactosidase activity of the riboswitch reporter in the presence (+) or absence ( $\Delta$ ) of PBP1 or treated with (+) 5 µg ml<sup>-1</sup> moenomycin (MOE). All cells lack disA, cdaS and cdaAR, and harbour an IPTG-regulated allele of cdaAR expressed with 50 µM IPTG. **e**, Representative immunoblots of B. subtilis cells expressing CdaA-His under IPTG-inducible control with 50 µM IPTG in the presence (+) or absence ( $\Delta$ ) of PBP1. SigA controls for loading. Molecular weight markers in kDa are indicated. **f**, Bar graph showing  $\beta$ -galactosidase activity from the riboswitch reporter in the indicated PBP1 depletion strain, with different concentrations of IPTG. Data are means  $\pm$  s.d. of 3 biological replicates (**b**,**c**,**d**,**f**).

similar amino acid content to CdaR's IDR. The characterized IDRs are thought to sense cell wall defects by entering gaps in the meshwork or through non-covalent interactions with the  $PG^{30}$ .

To investigate whether CdaR's IDR is involved in sensing or responding to cell wall defects<sup>32</sup>, we compared IPTG-regulated alleles of cdaA-cdaR (cdaAR) and a variant in which the IDR on CdaR was deleted ( $cdaAR\Delta ID$ ). Cells lacking all c-di-AMP cyclases are inviable, but cells expressing cdaAR or  $cdaAR\Delta ID$  grew similarly (Fig. 3c). However, upon deletion of PBP1, the cells expressing CdaRΔID had a severe growth defect compared with full-length CdaR (Fig. 3c). The difference in growth was also observed in the presence of moenomycin (Fig. 3d). Importantly, CdaR variants in which the order of amino acids in the IDR was scrambled were fully functional (Fig. 3c,d). Immunoblot analysis of functional His-tagged variants indicate that CdaR, CdaRΔID and the scrambled variants were all expressed at similar levels (Extended Data Fig. 3a and Supplementary Fig. 5b). CdaA-His was also present at similar levels in cells expressing CdaR or CdaRΔID (Extended Data Fig. 3b), and CdaR-His and CdaR∆ID-His stability was unchanged in the absence of PBP1 (Extended Data Fig. 3c). Finally, co-immunoprecipitation experiments indicate that the CdaA-CdaR complex was unaffected by the absence of CdaR's IDR (Extended Data Fig. 3d). To investigate whether the function of the IDR is conserved among CdaR homologues, we generated CdaR chimeras in which the native IDR was replaced with IDRs from Bacillus cereus and Enterococcus faecalis CdaRs (Fig. 3b).

We also tested the IDRs from B. subtilis RsgI and PBP1 that have been implicated in sensing cell wall defects $^{30}$ . In all cases, the CdaR chimeras supported growth in the absence of PBP1 (Fig. 3c). We conclude that the function of CdaR's IDR is likely to be conserved and involved in sensing and responding to cell wall defects.

The experiments described above were performed under sensitizing conditions in which CdaA and CdaR were co-expressed below their native levels (Extended Data Fig. 3e). To investigate the importance of CdaR's IDR at native expression levels, we analysed full-length CdaR and several variants in a strain lacking GpsB with reduced levels of PBP1. Expression of CdaR at native levels supported growth (Fig. 3e,f). By contrast, expression of CdaR $\Delta$ ID resulted in complete loss of viability (Fig. 3e,f). CdaR with a scrambled IDR or Rsgl's IDR restored growth in this background (Fig. 3e).

#### CdaR's IDR is required to modulate c-di-AMP levels

To determine whether CdaR's IDR is required to increase CdaA activity in the presence of cell wall stress, we used our riboswitch reporter to monitor c-di-AMP levels (Fig. 2a). Cells expressing CdaA and CdaR, CdaR $\Delta$ ID, or CdaR $\Delta$ ID-ID $_{scrt}$  at native levels (Extended Data Fig. 3e) were grown in the presence or absence of PBP1 and analysed for c-di-AMP levels. In the strain expressing full-length CdaR,  $\beta$ -galactosidase activity decreased in the absence of PBP1, reflecting an increase in c-di-AMP levels (Figs. 2d and 4a). By contrast, in cells expressing CdaR $\Delta$ ID,

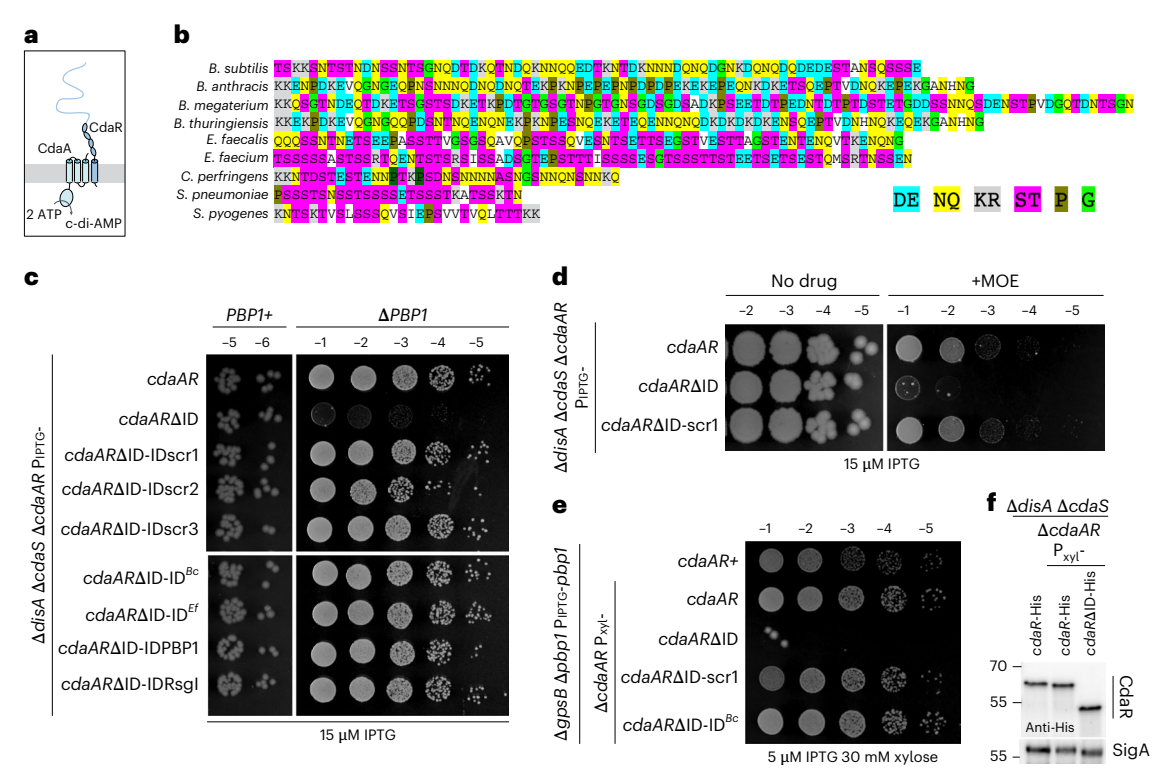


**Fig. 3** | **CdaR's IDR is important for cell envelope integrity. a**, Schematic diagram of CdaA and CdaR. CdaR's IDR is shown as a light blue wavy line. **b**, Representative IDRs on CdaR homologues from the indicated organisms. Residues with similar properties are coloured similarly. **c**, Spot dilutions of the indicated *B. subtilis* strains on LB agar with 15 μM IPTG in the presence or absence of PBP1. All cells lack *disA*, *cdaS* and *cdaAR*, and harbour an IPTG-regulated allele of *cdaAR*. *cdaR* alleles with scrambled (scr1–3) IDRs, chimeras with IDRs from CdaR homologues in *B. cereus* (ID<sup>Bc</sup>), *E. faecalis* (ID<sup>EF</sup>), *B. subtilis* PBP1 (ID<sub>PBP1</sub>) and *B. subtilis* Rsgl

 $(ID_{Rsgl}) \ are shown. \ \textbf{d}, Spot dilutions of the indicated strains on LB agar with 15 \ \mu M IPTG \ and 5 \ \mu g \ ml^{-1} \ MOE \ or no drug. \ \textbf{e}, Spot dilutions of the indicated strains on LB agar with 5 \ \mu M IPTG \ and 30 \ mM \ xylose. \ \textbf{f}, Representative immunoblots of the indicated \textit{B. subtilis} strains expressing CdaR-His at its native locus, or CdaR-His and CdaR \Delta ID-His at an ectopic locus under xylose-inducible control. Inducible variants were grown in the presence of 30 \ mM \ xylose. SigA controls for loading. Molecular weight markers in kDa are indicated. All experiments were performed in biological triplicate and a representative is shown.$ 

 $\beta$ -galactosidase activity was similar in the presence and absence of PBP1 (Fig. 4a). Importantly, the CdaR variant with the scrambled IDR phenocopied wild type. Similar results were obtained when the same set of strains were treated with moenomycin (Fig. 4b). These results argue that CdaR's IDR is important for the activation of CdaA-dependent c-di-AMP synthesis in response to cell wall defects.

#### Cyclic-di-AMP controls cellular turgor pressure

We next investigated whether changes in c-di-AMP levels impact cytoplasmic turgor pressure. To assess the acute effects of a rapid increase in c-di-AMP, we took advantage of a hyperactive allele (L44F) of the sporulation-specific c-di-AMP synthase cdaS<sup>3</sup>. Expression of cdaS(L44F) under the control of a strong IPTG-regulated promoter (P<sub>hv</sub>) inhibits colony formation (Fig. 5a) and inhibits growth in liquid medium within 30 min of induction (Extended Data Fig. 4a). At this timepoint, c-di-AMP levels are markedly higher (Extended Data Fig. 5a-c). We introduced this hyperactive allele into a strain harbouring cytoplasmic mCherry and a GFP fusion to a membrane protein (FB) to visualize the cytoplasmic membranes. We then imaged the cells by fluorescence microscopy before and at timepoints after the addition of IPTG. Within 15 min of induction, cytoplasmic mCherry no longer filled the entire cell, and the fluorescent membrane protein accumulated in the regions that lacked mCherry fluorescence (Fig. 5b). These phenotypes became more pronounced over time (Extended Data Fig. 4b). Similar results were obtained using the fluorescent membrane dye TMA-DPH (Extended Data Fig. 4c) instead of FB-GFP. We used transmission electron microscopy (TEM) to obtain a higher-resolution view of the cell ultrastructure. As can be seen in Fig. 5c, 15 min after IPTG induction, the cytoplasmic membranes had retracted from the cell envelope,

forming large invaginations in the cytosol (Fig. 5c and Extended Data Fig. 6). Membrane retraction can explain the absence of cytoplasmic mCherry and accumulation of FB-GFP, and is consistent with a rapid loss of cytoplasmic turgor pressure. In support of this idea, we found that cells treated with the phospholipid synthesis inhibitor cerulenin after cdaS(L44F) induction but before the onset of membrane invaginations still formed membrane patches that excluded cytoplasmic mCherry (Extended Data Fig. 7), indicating that the invaginations were not due to hyperactive membrane synthesis.

To more directly assess whether the membrane invaginations were due to a rapid drop in intracellular osmolarity and the resulting decrease in turgor, we induced cdaS(L44F) and, immediately before visualization, resuspended the cells in LB medium lacking NaCl (Extended Data Fig. 8a). The reduction in external osmolarity markedly reduced the formation of membrane invaginations (Extended Data Fig. 8b). Collectively, these experiments strongly suggest that increasing c-di-AMP reduces cellular turgor pressure.

To probe the effects of an acute decrease in c-di-AMP levels, we generated a hyperactive allele of the c-di-AMP phosphodiesterase gdpP that lacks its transmembrane and PAS domains. Overexpression of this allele using the same strong IPTG-regulated promoter  $P_{hy}$  prevented colony formation (Fig. 5a), inhibited growth in liquid medium within 45 min (Extended Data Fig. 9a), and rapidly decreased the cellular pool of c-di-AMP (Extended Data Fig. 5d,e). By fluorescence microscopy, we observed cell bulging followed by lysis starting at 45 min after induction (Fig. 5d and Extended Data Fig. 9b). We attribute the morphological changes and lysis to altered cell wall synthesis due to the massive increase in cytoplasmic turgor. Altogether, these data are consistent with acute changes in c-di-AMP impacting cellular turgor.

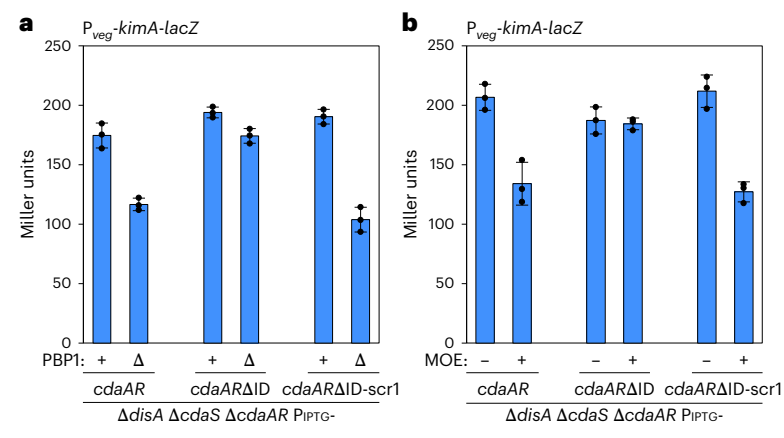


Fig. 4 | CdaR's IDR is required to modulate c-di-AMP levels in response to cell wall stress. Bar graphs showing β-galactosidase activity from the riboswitch (kimA) reporter in the indicated B. subtilis strains lacking disA, cdaS and cdaAR, and harbouring an IPTG-regulated allele of cdaAR,  $cdaAR\Delta$ ID, or  $cdaAR\Delta$ ID-

scr1 expressed with 50  $\mu$ M IPTG. Each strain was assayed in the presence (+) or absence ( $\Delta$ ) of PBP1 (**a**) and before or after treatment with (+) 5  $\mu$ g ml<sup>-1</sup>MOE (**b**) for 90 min. Data are means  $\pm$  s.d. of 3 biological replicates.

#### Chronic changes in c-di-AMP levels cause changes in turgor

To investigate the impact of chronic increase and decrease in c-di-AMP, we fused cdaS(L44F) to our standard IPTG-regulated promoter ( $P_{IPTG}$ ) and grew the cells in 500 µM IPTG (high c-di-AMP) and separately expressed cdaAR under the same IPTG-regulated promoter at low levels (5 µM IPTG) in a strain lacking the native cyclases (low c-di-AMP) (Fig. 5e,f). In liquid medium, these strains grew at rates similar to wild type, despite having higher and lower levels of c-di-AMP (Fig. 5e,f and Supplementary Fig. 7). We introduced orthogonal cytoplasmic reporters into these strains and wild type, and imaged a mixture of exponentially growing cultures of each. As can be seen in Fig. 5g,h, the strains had qualitatively and quantitatively distinct widths: cells with low c-di-AMP levels were chubby and cells with high c-di-AMP were skinny. Changes in cell size that inversely correlate with c-di-AMP levels as shown here have been reported previously in S. aureus, Mycobacterium tuberculosis and Borrelia burgdorferi<sup>33-35</sup>. Although these phenotypes are consistent with the idea that c-di-AMP levels impact cytoplasmic turgor, turgor pressure has never been measured in strains with different levels of this second messenger.

To qualitatively assess whether cells with chronically high c-di-AMP have reduced turgor pressure, we analysed their propensity to lyse after treatment with lysozyme. We mixed exponentially growing cells expressing *cdaS*(L44F) under control of our standard P<sub>IPTG</sub> promoter with wild-type cells and imaged them by time-lapse microscopy on an LB agar pad before and after adding lysozyme. To distinguish the two strains, the wild-type cells expressed cytoplasmic GFP and the CdaS(L44F)-producing cells expressed mCherry. As anticipated, within 5 min of lysozyme addition, most cells underwent lysis. However, a subset formed stable protoplasts (Fig. 5i). Consistent with the idea that cells with chronically high c-di-AMP have reduced turgor pressure, >2-fold more protoplasts were generated from cells with high c-di-AMP than wild type (Fig. 5j) and Supplementary Movie 1).

To directly and quantitatively measure turgor pressure in cells with different levels of c-di-AMP, we used an established microfluidics-based assay  $^{36,37}$ . First, the degree to which cells are inflated by turgor was determined by measuring cell length before and after acutely lysing them with detergent. In a separate experiment, cell length was measured in response to a series of hyperosmotic shocks, which reduce turgor pressure, to determine the shock magnitude ( $\Delta C$ ) that caused length to contract to its detergent-deflated value (Extended Data Fig. 10a). Combined, these data provide an empirical, quantitative measurement of turgor pressure in units of osmolarity, which can be converted to units of pressure using  $P = RT\Delta C$  (see Methods). For these experiments, we compared exponentially growing wild-type cells and

the strains described above with high and low c-di-AMP. As can be seen in Fig. 5k, cells with chronically low c-di-AMP had higher turgor pressure than wild-type, while cells with chronically high levels of c-di-AMP had lower turgor pressure than wild type (Extended Data Fig. 10b-d). We conclude that cells modulate cytoplasmic turgor by controlling the levels of c-di-AMP.

#### CdaAR-mediated decrease in turgor protects cells from lysis

With the knowledge that c-di-AMP controls cytoplasmic turgor pressure, we returned to our cell wall defective mutants to determine whether the CdaAR-mediated increase in c-di-AMP protects cells from lysis because of the reduction in turgor. To do so, we analysed the growth of our mutants in media with different osmolarities. The growth defect of cells expressing CdaRΔID in the absence of PBP1 was partially suppressed on medium with high osmolarity and enhanced on low-osmolarity medium (Extended Data Fig. 10e,f). Importantly, this mutant maintained low c-di-AMP levels (Extended Data Fig. 10g) when grown in the presence or absence of high-osmolarity medium, indicating that the suppression was due to reduced turgor from the change in external osmolarity rather than altered c-di-AMP levels. Similarly, the growth defect of cells lacking pbp1 and cdaAR or expressing cdaA(D171A) was suppressed in medium with high osmolarity (Extended Data Fig. 10h). Taken together, these results argue that the slow growth and cell envelope defects (Fig. 1c,d) associated with these double mutants are due to high cytoplasmic turgor and the resulting osmotic lysis. We conclude that the increase in c-di-AMP in cells lacking PBP1 protects cells from lysis by reducing turgor pressure.

#### **Discussion**

Altogether, our data define a signal transduction pathway that controls the intracellular pool of c-di-AMP and establishes a direct link between maintenance of the cell wall peptidoglycan and modulation of cytoplasmic turgor pressure. Our findings support a model in which CdaR's IDR senses defects in the PG meshwork and triggers the production of c-di-AMP by CdaA (Fig. 6). The rise in c-di-AMP inhibits osmolyte import and activates  $K^{+}$  export, thus decreasing intracellular osmolyte concentration and reducing turgor. This response protects the cell from autolysis and probably enables repair. Unlike the acute responses to the very high or very low levels of c-di-AMP reported here (Fig. 5b-d), the response to cell wall defects had a more modest impact on c-di-AMP levels (Fig. 2d-f) and therefore more modestly alters cytoplasmic turgor. We suspect that these changes are sufficient to prevent autolysis and are tuned by the extent of defects in the meshwork sensed by CdaR's IDR. Our data further argue that this signalling pathway is

shared among bacteria that possess a CdaR homologue with an IDR (Supplementary Fig. 4). The role of the more highly conserved YbbR repeats on CdaR is currently unknown but, on the basis of our findings, we suspect that it also monitors some aspect of the envelope and modulates turgor in response. More generally, we hypothesize that reducing cytoplasmic turgor in response to envelope stress is likely to be a common feature of many bacterial phyla beyond those that possess CdaAR and/or c-di-AMP.

The mechanism by which CdaR's IDR monitors the PG meshwork is currently unknown. However, our previous studies of the IDRs on the anti-sigma factor RsgI and the cell wall synthase PBP1 suggest that these regions may enter gaps in the meshwork and generate a mechanotransducive pulling force. In the case of RsgI, this force dissociates the autocleaved ectodomain of the anti-sigma factor, triggering intramembrane proteolysis of its membrane-anchored portion and activation of its cognate Sigma-I transcription factor 30,38. For PBP1, we suspect that the pulling force stabilizes an active conformation of the polymerase 39. By analogy, we propose that a pulling force exerted on CdaR causes a conformational change that activates CdaA, either allosterically or by changing its multimerization state.

It is noteworthy that the cell wall defects that CdaR responds to result from impaired synthesis by the class A PBPs (aPBPs), such as PBP1. Among all the cell wall targeting antibiotics tested, only moenomycin stimulated c-di-AMP production (Extended Data Fig. 2b). The aPBPs are thought to fortify the cell wall by synthesizing peptidoglycan between the circumferential glycan strands generated by SEDS-bPBP enzymes in the elongasome<sup>16</sup>. Evidence suggests that the aPBPs play a critical role in stitching these hoop-like strands together. Our findings that both CdaA-CdaR and RsgI-SigI act homeostatically support the idea that the IDRs evolved to monitor the wall for places where the aPBPs failed to generate a continuous meshwork. Detection of these gaps by RsgI's IDR activates the SigI regulon to increase cell wall biogenesis, detection by CdaR's IDR reduces turgor pressure, and PBPI's IDR directs the synthase to the places that require fortification.

Interestingly, a meta-analysis of all the genes that are located downstream of the *kimA* riboswitch revealed that the largest class (>45%) are genes with Clusters of Orthologous Groups functions assigned to cell envelope biogenesis<sup>11,12,40</sup>. The vast majority of these c-di-AMP-regulated genes encode PG hydrolases and are mainly found in actinobacterial genomes. Since *kimA* is an off-riboswitch, an increase

in c-di-AMP levels would result in a reduction in expression of these cell wall cleaving enzymes. By analogy to what we have discovered in *B. subtilis*, we hypothesize that cell wall defects in these actinobacteria increase c-di-AMP levels, resulting in both a reduction in turgor pressure 41,42 and PG hydrolase production. Together, these responses would protect cells from autolysis.

Clinically relevant strains of S. aureus that have increased tolerance or resistance to β-lactam antibiotics often contain mutations in the phosphodiesterase gdpP that chronically increase c-di-AMP levels<sup>20,43-47</sup>. The mechanisms underlying these phenomena has been unclear. Our discovery that B. subtilis cells with chronically high levels of c-di-AMP have reduced cytoplasmic turgor pressure provides a plausible explanation for the increased antibiotic tolerance and resistance in the S. aureus mutants. However, our analysis of turgor pressure revealed a second potential contribution to these phenomena. Specifically, cells with chronically high levels of c-di-AMP had nonlinear pressure-elongation curves (Extended Data Fig. 10d) whereby for hyperosmotic shocks less than 800 mM the cells barely contracted in length, compared with the linear force extension curves observed in wild type and cells with low c-di-AMP (Extended Data Fig. 10b,c). This indicates that cells with chronically high c-di-AMP have cell envelopes with increased stiffness across this pressure range<sup>48</sup>. We hypothesize that these properties arise from changes in the cell wall microstructure as a result of PG synthesis at reduced turgor pressure. Thus, if S. aureus cells respond similarly to chronically high c-di-AMP, then a reduction in turgor and stiffening of the cell wall could both contribute to the increased tolerance and resistance associated with  $\Delta gdpP$  mutants.

Modulating cytoplasmic turgor pressure represents an attractive mechanism to respond to intracellular and extracellular stress. In addition to cell wall defects, stresses that are thought to alter c-di-AMP levels include changes in external osmolarity, DNA damage and altered metabolism<sup>1,49–51</sup>. In the latter two cases, the role for altered turgor is less clear. One possibility is that increasing turgor in response to DNA damage might prevent or slow constriction of the cytokinetic ring to ensure repair of the chromosomal lesion before division. In the case of metabolic flux, if changes in metabolism impact PG precursor synthesis, this could be balanced by reduced turgor to slow elongation or prevent autolysis. The challenge for the future is to define the full set of signals and transduction pathways that regulate the cellular pools

Fig. 5 | c-di-AMP controls cytoplasmic turgor pressure. a, Spot dilutions of the indicated strains on LB agar supplemented with 500 µM or no IPTG. B. subtilis strains contain the  $P_{spank}(P_{IPTG})$  or  $P_{hyperspank}(P_{hy})$  promoter fused to the cdaS(L44F) allele or the gdpP(cyto) allele lacking its TM and PAS domains. b, Representative fluorescence and phase-contrast images of B. subtilis cells with  $P_{hv}$ -cdaS(L44F) grown in LB before and 15 min after addition of 500  $\mu$ M IPTG. At 15 min after induction, cells were pelleted, spotted onto LB agarose pads and imaged ~5 min after collection. Cells contain mCherry and SpoIVFB-GFP(FB-GFP) for cytoplasmic and membrane labelling. Sites of membrane accumulation and cytoplasmic gaps are indicated (yellow triangles). Treatment of cells with the fatty acid kinase inhibitor cerulenin 10 min after IPTG addition did not prevent membrane accumulation (Extended Data Fig. 7), indicating that this phenotype is not due to an uncoupling of phospholipid and cell wall synthesis. c, Transmission electron micrographs of the cells visualized in **b**. Cells were immediately fixed after collection. Scale bar, 100 nm. d, Representative overlaid phase-contrast and fluorescence images of B. subtilis cells with P<sub>hv</sub>-gdpP(cyto) and cytoplasmic mCherry before and 60 min after addition of 500  $\mu$ M IPTG. Bulging (yellow triangles) and lysed (white triangles) cells are indicated. e, Bar graph showing  $\beta$ -galactosidase activity from the kimA riboswitch reporter. LOW cells ( $\Delta disA$  $\Delta cdaS \Delta cdaAR P_{IPTG}$ -cdaAR) were grown with 5  $\mu$ M IPTG; wild-type (WT); HIGH cells (P<sub>IPTG</sub>-cdaS(L44F)) were grown with 500 μM IPTG. **f**, Bar graph showing c-di-AMP levels as measured by ELISA assay in the same strains and conditions as in  $\boldsymbol{e}.$  Values were normalized to the  $OD_{600}$  of the culture. Data are means  $\pm$  s.d. of 3 biological replicates (e,f). g, Overlaid fluorescence and phase-contrast images of the strains in e. LOW cells contain mTag-BFP, WT contains GFP, and HIGH cells

contain mCherry. The strains were grown in their respective IPTG concentrations and mixed before imaging. h, Cell width quantification of the cells described in e.  $Each \ contained \ cytoplasmic \ mCherry \ for \ quantification \ (Supplementary \ Fig. \ 8).$ Large circles represent the mean width of ≥40 cells from at least 5 fields of view. Shades of red, blue and green are measurements from 3 biological replicates. \*P < 0.05, NS, not significant; two-tailed Student's t-test. The P values are 0.15 between LOW and WT, 0.034 between WT and HIGH, and 0.043 between LOW and HIGH, i. Overlaid fluorescence and phase-contrast images from a time-lapse movie of WT (with GFP) and HIGH (with mCherry) as described in e. Exponentially growing cells were mixed and spotted onto an LB agarose pad. Lysozyme was added to the back of the pad and cells imaged over 20 min (Supplementary Movie 1). Timepoints 0 and 13 min after lysozyme addition are shown. Examples of protoplasts that have not lysed (red and green triangles) are highlighted. i, Quantification of the percent survival for each cell type after 20 min of lysozyme treatment relative to the number of initial cells in the region of interest shown in **h**. n = 496 cells (224 HIGH + 272 WT). These data are representative of 3 biological replicates and one is shown. k, Bar graphs showing measurements of the cytoplasmic turgor pressure of the LOW, WT and HIGH strains described above (see Methods). The pressure values were calculated from the regression of the osmotic force extension curve for each strain (Extended Data Fig. 10b-d). The error bars show the propagation error as calculated from the regression and lysis error (see Methods). The number of cells analysed under each condition is reported in Extended Data Fig. 10. All microscopy was performed in biological triplicate and representative images are shown. Scale bars (b,d,g,i), 5 µm.

of c-di-AMP and to understand how modulating cytoplasmic turgor functions to manage these stresses.

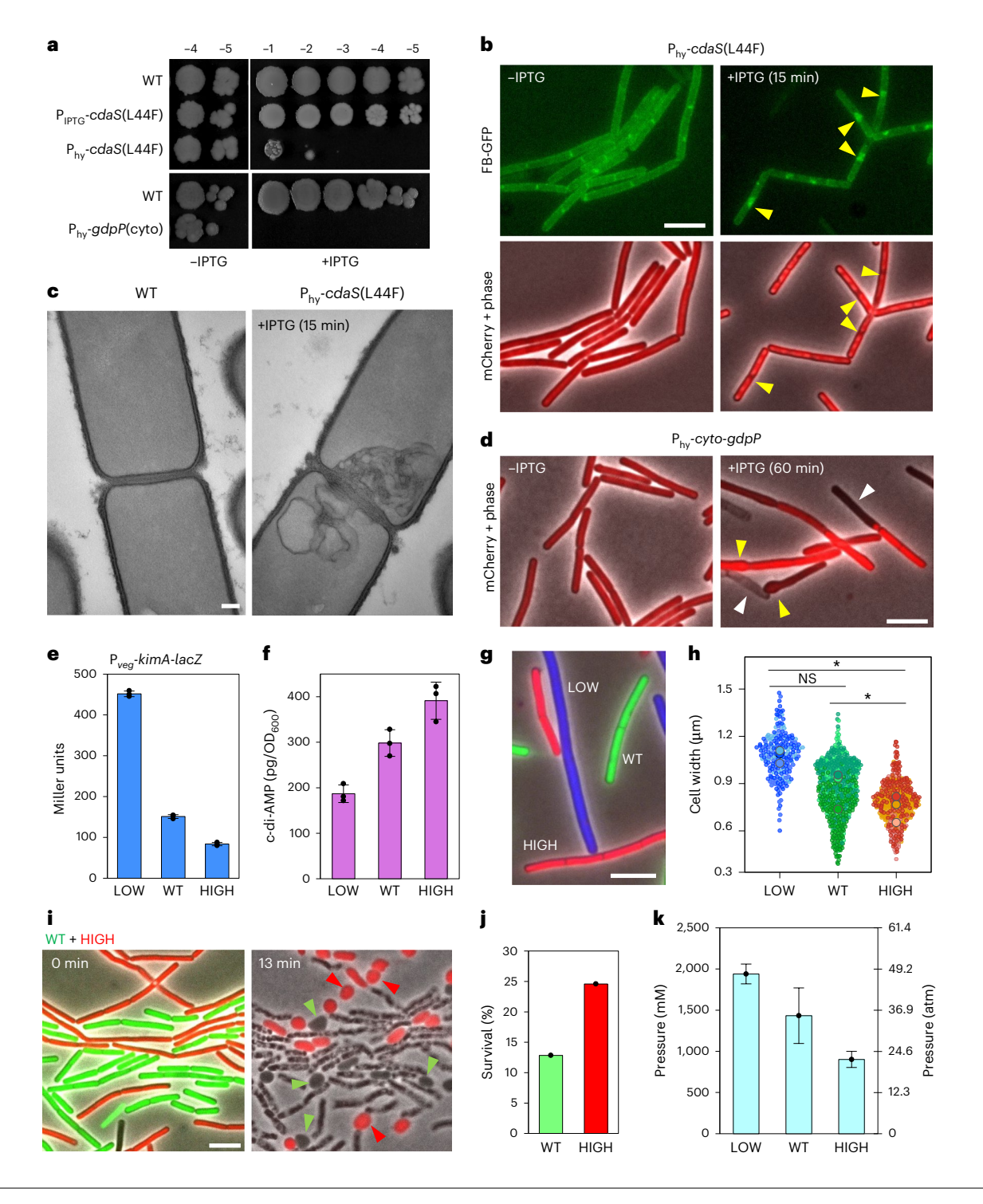
#### Methods

#### General methods

All *B. subtilis* strains were derived from the prototrophic strain PY79 (ref. 52). Unless otherwise indicated, cells were grown in LB medium  $^{53}$  at  $37\,^{\circ}\text{C}$  with aeration. For all experiments, single freshly streaked colonies were subcultured for 3 h at  $37\,^{\circ}\text{C}$  before back dilution and growth to mid-log phase with aeration at  $37\,^{\circ}\text{C}$ . Antibiotic concentrations used were:  $100~\mu g~\text{ml}^{-1}$  spectinomycin,  $10~\mu g~\text{ml}^{-1}$  kanamycin,  $5~\mu g~\text{ml}^{-1}$  chloramphenicol,  $10~\mu g~\text{ml}^{-1}$  tetracycline,  $1~\mu g~\text{ml}^{-1}$  erythromycin and  $25~\mu g~\text{ml}^{-1}$  lincomycin.

#### **Strain construction**

Insertion–deletion mutants were generated by isothermal assembly<sup>54</sup> of PCR products followed by direct transformation into *B. subtilis* using a one-step competence method. All deletions were confirmed by PCR. Antibiotic cassette removal was performed using a temperature-sensitive plasmid that constitutively expresses Cre recombinase<sup>55,56</sup>. Ectopic integration constructs were cloned in *E. coli* followed by transformation into *B. subtilis*. Unmarked insertions and point mutations were made via allelic exchange with the vector pminiMAD2 (ref. 57). Tables of strains, plasmids and oligonucleotide primers, and a description of strain and plasmid construction can be found online as supplementary data (Supplementary Tables 1–4 and Supplementary Information).



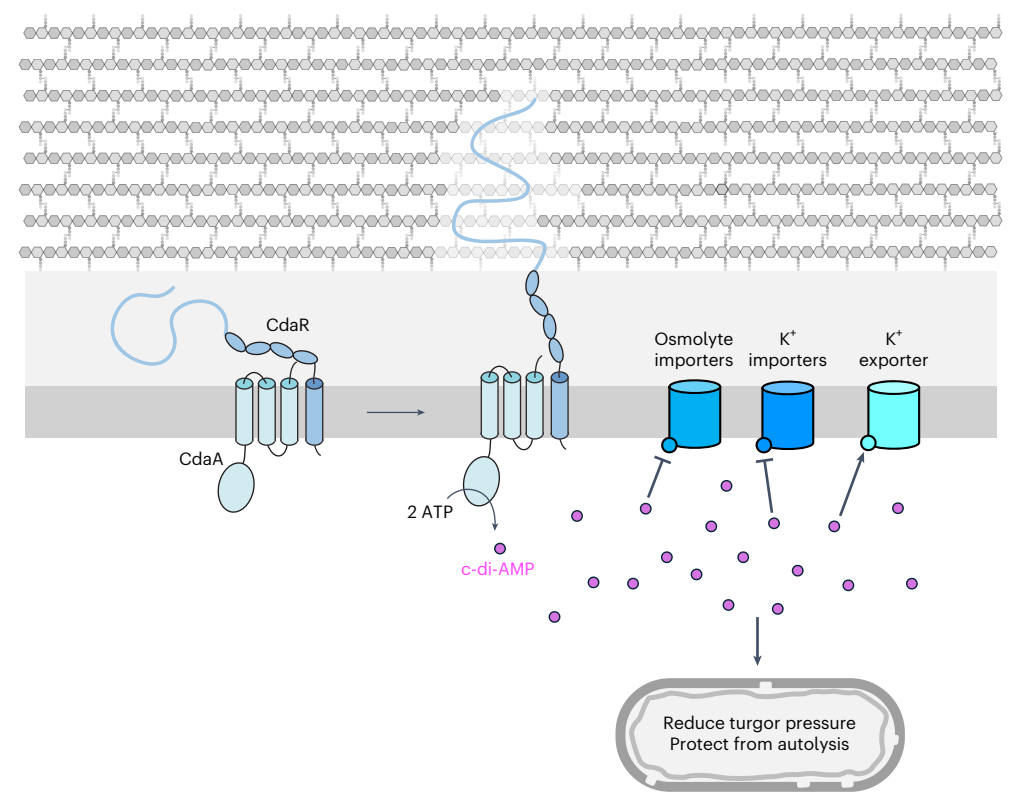


**Fig. 6 | Schematic model of the CdaAR signalling pathway.** CdaR's intrinsically disordered region (squiggly blue line) senses defects in the cell wall meshwork, leading to a conformational change in the CdaAR complex that stimulates CdaA activity. Increased c-di-AMP molecules (pink circles) bind to cytoplasmic domains (blue circles)<sup>8</sup> on membrane transporters. C-di-AMP binding inhibits

 $K^*$  and osmolyte importers, and activates  $K^*$  exporters. The reduction in cytoplasmic osmolarity reduces cellular turgor pressure. Reduced turgor protects the cell from lysis and could enable fortification of the meshwork. In the absence of cell wall stress, the IDR resides in the Gram-positive periplasm<sup>68</sup>.

#### Statistics and reproducibility

All experiments were carried out in biological triplicate unless otherwise indicated. Bar graphs show the individual replicates, with error bars representing the average and standard deviation across biological replicates. For fluorescence microscopy, all experiments were carried out in biological triplicate, and at least 10 fields of view imaged and analysed when quantified. Time-course TEM images are representatives from two biological replicates.

#### **β**-galactosidase assays

*B. subtilis* strains were grown in LB medium at 37 °C to an OD<sub>600</sub> of ~0.5. The optical density was recorded and 1 ml of culture was collected and assayed for β-galactosidase activity as previously described <sup>58</sup>. Briefly, cell pellets were resuspended in 1 ml Z buffer (40 mM NaH<sub>2</sub>PO<sub>4</sub>, 60 mM Na<sub>2</sub>HPO<sub>4</sub>, 1 mM MgSO<sub>4</sub>, 10 mM KCl and 50 mM β-mercaptoethanol). Of this suspension, 250 μl was added to 750 μl of Z buffer supplemented with lysozyme (0.25 mg ml<sup>-1</sup>), and the samples were incubated at 37 °C for 15 min. The colorimetric reaction was initiated by addition of 200 μl of 2-nitrophenyl-β-D-galactopyranoside (ONPG, 4 mg ml<sup>-1</sup>) in Z buffer and stopped with 500 μl 1 M Na<sub>2</sub>CO<sub>3</sub>. The reaction time and the absorbance at 420 nm and OD<sub>550</sub> of the reactions were recorded, and the β-galactosidase specific activity in Miller units was calculated according to the formula [ $A_{420}$ –1.75 × (OD<sub>550</sub>)]/(time [min] × OD<sub>600</sub>) × dilution factor × 1,000 (ref. 59). Plots were generated using Excel or Graphpad Prism.

#### Immunoblot analysis

Immunoblot analysis was performed as described previously  $^{60}$ . Briefly, 1 ml of exponentially growing culture (OD $_{600}$  ~ 0.5) was collected and resuspended in lysis buffer (20 mM Tris pH7.0, 10 mM MgCl $_2$  and 1 mM EDTA, 1 mg ml $^{-1}$  lysozyme, 10  $\mu g$  ml $^{-1}$  DNase I, 100  $\mu g$  ml $^{-1}$  RNase A,

 $1 \,\mathrm{mM\,PMSF}$ ) to a final OD<sub>600</sub> of 10 for equivalent loading. The cells were incubated at 37 °C for 15 min, followed by addition of an equal volume of Laemmli sample buffer (0.25 M Tris pH 6.8, 4% SDS, 20% glycerol, 10 mM EDTA) containing 10% β-mercaptoethanol. Samples were heated for 15 min at 65 °C before loading. Proteins were resolved by SDS-PAGE on 12.5% polyacrylamide gels, electroblotted onto Immobilon-P membranes (Millipore) and blocked in 5% non-fat milk in phosphate-buffered saline (PBS) with 0.5% Tween-20. The blocked membranes were probed with anti-SigA (1:10,000)<sup>61</sup>, anti-EzrA (1:10,000)<sup>62</sup>, anti-His (1:4,000) (GenScript) and anti-HA (1:1,000) (Sigma) antibodies diluted into 3% BSA in PBS with 0.05% Tween-20. Primary antibodies were detected using horseradish peroxidase-conjugated goat anti-rabbit or anti-mouse IgG (BioRad) and the Super Signal chemiluminescence reagent as described by the manufacturer (Pierce). Signal was detected using a Bio-Techne FluorChem R System. Images were cropped and contrast adjusted using Fiji.

#### Co-immunoprecipitation

A volume of 100 ml of exponentially growing *B. subtilis* cultures  $(OD_{600} \sim 0.5)$  expressing CdaA-His6 with 500  $\mu$ M IPTG and CdaR-HA with 20 mM xylose were collected  $(3,000\,g,10\,\text{min})$  and washed twice in SMM medium  $(0.5\,\text{M}\,\text{sucrose},20\,\text{mM}\,\text{MgCl}_2,20\,\text{mM}\,\text{maleic}$  acid pH 6.5) before resuspension in 10 ml SMM + 0.5 mg ml<sup>-1</sup> lysozyme + 5 U ml<sup>-1</sup> mutanolysin. Cells were rotated for 45 min at room temperature and monitored for protoplasting by light microscopy. Protoplasts were pelleted  $(3,000\,g,10\,\text{min})$  and washed once in SMM before lysing in 10 ml cold hypotonic buffer  $(20\,\text{mM}\,\text{HEPES-NaOH}\,\text{pH}\,8,200\,\text{mM}\,\text{NaCl},1\,\text{mM}\,\text{dithiothreitol},1\,\text{mM}\,\text{PMSF},EDTA\,\text{complete}\,$  (Roche)). Lysates were supplemented with 1 mM MgCl<sub>2</sub> and CaCl<sub>2</sub>, 125 U benzonase and 20  $\mu$ g ml<sup>-1</sup> RNase A, followed by incubation

on ice for 30 min. Lysates were subjected to ultracentrifugation at  $100.000 \times g$  for 1 h at 4 °C. The supernatant was removed and the membrane pellet dispersed in 900 µl buffer G (20 mM HEPES-NaOH pH 8, 200 mM NaCl, 1 mM dithiothreitol, 10% (v/v) glycerol). To solubilize the membrane proteins. 100 μl of 10% n-dodecyl-β-p-maltoside (DDM) was added to the membrane fraction and the mixture rotated for 1 h at 4 °C. The soluble and insoluble material were separated by ultracentrifugation at  $100,000 \times g$  for 1 h at 4 °C. The supernatant containing detergent-solubilized proteins was mixed with anti-His resin (Genscript) and rotated for 2 h at 4 °C. The resin was pelleted (3,000 g, 1 min) at 4 °C and washed 4× with 1 ml buffer G + 0.1% DDM, with 2 min of rolling at 4 °C between washes. The washed resin was resuspended in 50 µl 1× Laemmli sample buffer (0.25 M Tris pH 6.8, 4% SDS, 20% glycerol, 10 mM EDTA) and heated for 15 min at 50 °C. The resin was pelleted and supernatant transferred to a fresh tube before adding β-mercaptoethanol to a final concentration of 10%. The load and IP fractions were analysed by immunoblot as described above.

#### **Growth curves**

Cells were cultured to mid-log phase (OD $_{600}$  ~ 0.5) in LB containing indicated IPTG concentrations and back diluted into LB at the indicated IPTG concentrations at OD $_{600}$  = 0.005. When media contained antibiotics, the concentration was 0.5× the minimum inhibitory concentration (MIC, as determined by an MIC assay). Diluted culture containing antibiotics was added in technical triplicate to clear polystyrene 96-well plates (Genesee), and plates were incubated at 37 °C with shaking at 432 r.p.m. in an Infinite M Plex microplate reader (Tecan) for 18 h. The OD $_{600}$  was monitored every 5 min. OD $_{600}$  measurements were averaged at each timepoint across the technical triplicates and plotted using Excel.

#### **Spot titres**

Cells were cultured to late-log phase in permissive conditions, washed  $3\times$  in LB, normalized to  $OD_{600}$  = 1.5 and diluted 10-fold in LB to  $10^{-6}$ . Of each dilution, 5.5  $\mu l$  was spotted onto LB agar supplemented with the indicated IPTG and xylose concentrations. Plates were incubated at 37 °C for 16 h before imaging. Images were adjusted to greyscale using photoshop.

#### Fluorescence microscopy

Fluorescence microscopy was performed on a Nikon Ti2-E inverted microscope equipped with a Plan Apo ×100/1.45 phase-contrast oil objective and a Hamamatsu ORCA-Flash4.0 V3 Digital CMOS camera. Light was delivered with the Lumencor Spectra III Light Engine containing the following filters: 390/22, 440/20, 475/28, 510/25, 555/28, 575/25, 637/12, 748/12. Images were acquired using the Nikon Elements 5.2 acquisition software. Cells were cultured to mid-log phase ( $OD_{600} \sim 0.5$ ), 1 ml of culture was collected (4,000 g, 5 min) and concentrated into 50 µl LB, and 5.5 µl of concentrated culture were immobilized using 2% agarose pads containing LB medium. For samples imaged during an induction time course, image acquisition occurred ~5 min after collection due to procedures of cell concentration, mounting on agarose pads and setting up of the imaging. During this 5-min period, the production or degradation of c-di-AMP probably continued. Envelope integrity was monitored using 5 μM PI (Sigma), and membranes were detected using either the GFP-tagged membrane protein SpoIVFB<sup>58</sup> or the probe TMA-DPH at 50 µM (Fisher Scientific). Cytoplasm was labelled with constitutively expressed GFP, mCherry or mTag-BFP. Exposure times were 200 ms, 30 ms and 500 ms for cytoplasmic mCherry, GFP and mTag-BFP, respectively. Exposure times were 25 ms, 200 ms, 30 ms and 25 ms for phase, PI, SpoIVFB-GFP and TMA-DPH, respectively. Images were cropped and adjusted using Fiji. All images shown side by side were acquired, analysed and adjusted identically for comparison. Images are shown at a magnification of ×100 and cropped to 26 μm × 26 μm, unless otherwise indicated.

#### Cell width and %PI-positive quantification

Width quantification was performed using MicrobeJ<sup>63</sup> on cells expressing cytoplasmic mCherry or GFP. The settings were as follows: background = dark, thresholding = -50, area = 0-0, length = 1-30, width = 0.3-2, all other settings = default. All width measurements are representative of at least 70 cells and were quantified in biological triplicate. Plots were generated using superviolin (https://superviolin.streamlit.app/). Percent PI-positive cells were manually quantified using cytoplasmic GFP and PI as indicators for cell boundaries. %PI measurements are representative of at least 1,000 cells per biological replicate. Plots were generated using Excel.

#### Time-lapse microscopy after lysozyme treatment

BAB1505 and 1509 were cultured to mid-log phase (OD $_{600}$  ~ 0.5) in LB with O and 500  $\mu$ M IPTG, respectively. Equal ODs of cells were combined, and cells were pelleted (4 min, 5,000 g) and resuspended in 50  $\mu$ l LB. Volumes of 5.5  $\mu$ l of cells were spotted onto a 2% LB agarose pad in a dish coverslip. Just before imaging, 5  $\mu$ l of 2 mg ml $^{-1}$ lysozyme was spotted onto the back of the pad. Cells were imaged every 20 s for 20 min. The experiment was repeated in biological triplicate and representative images are shown. Although the percentage of total protoplasting varied between replicates, the ratio of high to wild-type c-di-AMP-containing protoplasts remained consistently >2-fold.

#### **Turgor pressure measurements**

For all measurements, bacteria were subcultured to mid-log phase in LB medium before back dilution into LB and loading into a microfluidic plate (BAO4, CellAsics, Millipore-Sigma) controlled by the ONIX microfluidic platform. Before loading into the microfluidic perfusion chamber, cells were incubated in the loading well of the microfluidic plate for 30 min at 37 °C to ensure steady-state growth. Time-lapse movies were performed on a Nikon Eclipse Ti2 inverted epifluorescence microscope with an oil-immersion ×100 objective (NA 1.40) and a BSI sCMOS camera. Cell tracking and analysis were performed using custom MATLAB scripts<sup>37</sup>. LB was supplemented with the indicated concentration of IPTG. At least 70 cells were analysed for each strain and condition. All experiments were performed in biological triplicate.

**Calculation of lysis strain.** Length contraction experiments were performed in a microfluidic device and imaged by phase-contrast microscopy. After loading cells into the microfluidic perfusion chamber, cells were perfused with LB medium for 5 min, followed by LB supplemented with 5% *N*-lauroylsarcosine for 2 min, to lyse cells. Finally, the perfusion media were switched back to LB to remove detergent. The lysis strain  $(\varepsilon_i)$  was calculated using the equation  $\varepsilon_i = (l_i - l_f)/l_i$  where  $l_i$  is the cell length before lysis and  $l_f$  is the cell length after lysis.

**Osmotic force extension assays.** The cells were loaded into the microfluidic chamber and consecutive osmotic shocks were performed by perfusing LB supplemented with the indicated concentrations of sorbitol. Typically, osmotic shocks were performed every 5 min for a duration of 3 min each. Alexa Fluor 647 dye was added to specific media to track medium switching. To calculate the change in length resulting from each osmotic shock, we determined the interval of each shock when the medium was exchanged. Then, for every cell, we calculated the longitudinal strain during each shock using the formula  $\varepsilon_i = (l_i - l_f)/l_i$ , where  $l_i$  is the length of the cell at the beginning of the interval and  $l_f$  is the maximum length of the cell during the interval.

**Pressure measurements.** Turgor pressure measurements were performed as previously described<sup>36</sup>. In brief, osmotic force extension experiments were combined with measurements of lysis strain. The pressure in units of osmolarity was calculated from the regression of the osmotic force extension curves, as the hyperosmotic shock magnitude that caused contraction of the cell wall to the rest length observed upon

lysis. The propagation error of the measurement was calculated using the formula  $\sigma_f \approx |f| \sqrt{((\sigma_a/A)^2 + \sigma_\beta/B)^2 - 2(\sigma_{a\beta}/AB)}$  where  $\sigma_a$  is the standard deviation of the lysis strain, A is the lysis strain,  $\sigma_\beta$  is the standard error of the regression, and B is the slope of the regression. The pressure in units of atm was calculated using the equation  $P = RT\Delta C$  where R is the gas constant, T the temperature, and  $\Delta C$  the osmolarity differential between pre and post osmotic shock.

#### Measurement of c-di-AMP

Volumes of 10 or 25 ml of exponentially growing *B. subtilis* cultures (OD $_{600}$  ~ 0.5) were collected by centrifugation (10 min, 3,000 g), washed in lysis buffer (50 mM HEPES-NaOH pH 7, 160 mM NaCl) and resuspended in 750  $\mu$ l lysis buffer. The lysis buffer was determined to be of identical osmolarity to LB using a Touch Micro Osmette (Precision Systems). Cells were lysed using a FastPrep Bead beater (MP Biomedical) and a 30- $\mu$ l sample was removed for protein concentration quantification. Lysates were heated at 95 °C for 10 min, clarified by centrifugation (3 min, 20,000 g), and the supernatant stored at –20 °C. Protein concentration was determined using Pierce Bradford Plus protein assay reagent (ThermoFisher).

ELISAs were performed using the Cayman c-di-AMP ELISA kit according to manufacturer instructions. Samples were diluted 10-fold into Immunoassay C buffer for measurement, and all samples were measured in biological and technical triplicate. The signal was read out at  $A_{450}$  using an Infinite M Plex microplate reader (Tecan).

#### Transmission electron microscopy

Of exponentially growing cells, 200 µl were washed once in LB, then immediately mixed with 200 µl 2× fixing solution (1.25% formaldehyde, 2.5% glutaraldehyde, 0.03% picric acid in 0.1 M sodium cacodylate buffer, pH 7.4) and immediately pelleted (6,800 g, 2 min). Samples were fixed at 4 °C overnight and then washed 3× in cacodylate buffer. The pellet was post fixed in 1% osmium tetroxide/1.5% potassium ferrocyanide for 1 h, washed 3× in water, incubated in 1% uranyl acetate (in water) for 1 h, and again washed 3× in water. Samples were dehydrated in increasing ethanol concentrations (50%, 75%, 95%, 100%) for 15 min each and incubated with propylene oxide for 1 h before embedding in epon mixed 1:1 with propylene oxide. Samples were allowed to polymerize at 60 °C for 48 h. Samples were sectioned and images were acquired on a JEOL 1200EX TEM equipped with an AMT XR111 (11 megapixel) CCD camera. For time course imaging, samples were taken just before induction (t = 0 min) and at the indicated timepoints after induction. For non-induced samples, samples were taken at mid-exponential phase.

#### **Osmolarity measurements**

Volumes of 30  $\mu$ l of media were assayed using a Touch Micro Osmette osmometer (Precision Systems). The system was calibrated before each set of measurements.

#### Multiple sequence alignment

Multiple sequence alignments were generated using Clustal Omega<sup>64</sup>.

#### **Bioinformatics analysis**

A local psi-blast run was performed on the amino acid sequence of *B. subtilis* CdaR against the RefSeq select database using 6 iterations and an *e*-value cut-off of 0.05 (ref. 65). The resulting sequences were analysed using IUPRED3 (ref. 66). If the disorder prediction was >0.5 for the final 20 amino acids or more, the protein was classified as IDR containing. Taxids of all CdaR homologues and IDR-containing homologues were used to plot onto a phylogenetic tree of 5,767 unique bacterial taxa. The tree was constructed using iTOL<sup>67</sup>.

#### **Reporting summary**

Further information on research design is available in the Nature Portfolio Reporting Summary linked to this article.

#### **Data availability**

No large-scale datasets were generated over the course of this study. All relevant data are available in the supplementary material. Raw data for all graphs and uncropped immunoblots have been uploaded as source data. Primers, synthetic DNA constructs and strains used can be found in supplementary tables. The RefSeq database downloaded from NCBI (https://ftp.ncbi.nih.gov/refseq/release/) as of June 2019 was used for the described bioinformatics analysis. The phylogenetic tree was generated from 5,767 unique bacterial taxa assembled from the assembled reference genomes in the prokaryotic RefSeq database as of June 2019. Source data are provided with this paper.

#### References

- Oberkampf, M. et al. c-di-AMP signaling is required for bile salt resistance, osmotolerance, and long-term host colonization by Clostridioides difficile. Sci. Signal. 15, eabn8171 (2022).
- Corrigan, R. M., Bowman, L., Willis, A. R., Kaever, V. & Gründling, A. Cross-talk between two nucleotide-signaling pathways in Staphylococcus aureus. J. Biol. Chem. 290, 5826–5839 (2015).
- Mehne, F. M. P. et al. Cyclic di-AMP homeostasis in *Bacillus* subtilis: both lack and high level accumulation of the nucleotide are detrimental for cell growth. *J. Biol. Chem.* 288, 2004–2017 (2013)
- Devaux, L. et al. Cyclic di-AMP regulation of osmotic homeostasis is essential in Group B Streptococcus. PLoS Genet. 14, e1007342 (2018).
- 5. Witte, C. E. et al. Cyclic di-AMP is critical for *Listeria* monocytogenes growth, cell wall homeostasis, and establishment of infection. *mBio* **4**, e00282-13 (2013).
- Stülke, J. & Krüger, L. Cyclic di-AMP signaling in bacteria. Annu. Rev. Microbiol. 74, 159–179 (2020).
- 7. Gundlach, J. et al. Control of potassium homeostasis is an essential function of the second messenger cyclic di-AMP in *Bacillus subtilis*. Sci. Signal. **10**, eaal3011 (2017).
- Gundlach, J. et al. Sustained sensing in potassium homeostasis: cyclic di-AMP controls potassium uptake by KimA at the levels of expression and activity. J. Biol. Chem. 294, 9605–9614 (2019).
- Fuss, M. F. et al. Cyclic di-AMP traps proton-coupled K<sup>\*</sup> transporters of the KUP family in an inward-occluded conformation. *Nat. Commun.* 14, 3683 (2023).
- Cereija, T. B., Guerra, J. P. L., Jorge, J. M. P. & Morais-Cabral, J. H. c-di-AMP, a likely master regulator of bacterial K⁺ homeostasis machinery, activates a K⁺ exporter. Proc. Natl Acad. Sci. USA 118, e2020653118 (2021).
- Nelson, J. W. et al. Riboswitches in eubacteria sense the second messenger c-di-AMP. Nat. Chem. Biol. 9, 834–839 (2013).
- Block, K. F., Hammond, M. C. & Breaker, R. R. Evidence for widespread gene control function by the ydaO riboswitch candidate. J. Bacteriol. 192, 3983–3989 (2010).
- Foster, A. J., van den Noort, M. & Poolman, B. Bacterial cell volume regulation and the importance of cyclic di-AMP. *Microbiol. Mol. Biol. Rev.* 88, e00181-23 (2024).
- Commichau, F. M., Gibhardt, J., Halbedel, S., Gundlach, J. & Stülke, J. A delicate connection: c-di-AMP affects cell integrity by controlling osmolyte transport. *Trends Microbiol.* 26, 175–185 (2018).
- Rohs, P. D. A. & Bernhardt, T. G. Growth and division of the peptidoglycan matrix. *Annu. Rev. Microbiol.* 75, 15.1–15.22 (2021).
- 16. Cho, H. et al. Bacterial cell wall biogenesis is mediated by SEDS and PBP polymerase families functioning semi-autonomously. *Nat. Microbiol.* **1**, 16172 (2016).
- Luo, Y. & Helmann, J. D. Analysis of the role of Bacillus subtilis σM in β-lactam resistance reveals an essential role for c-di-AMP in peptidoglycan homeostasis. Mol. Microbiol. 83, 623–639 (2012).

- Corrigan, R. M., Abbott, J. C., Burhenne, H., Kaever, V. & Gründling, A. c-di-AMP is a new second messenger in Staphylococcus aureus with a role in controlling cell size and envelope stress. PLoS Pathog. 7, e1002217 (2011).
- Kobras, C. M. et al. Loss of Pde1 function acts as an evolutionary gateway to penicillin resistance in Streptococcus pneumoniae. Proc. Natl Acad. Sci. USA 120, e2308029120 (2023).
- Banerjee, R., Gretes, M., Harlem, C., Basuino, L. & Chambers, H. F. A mecA-negative strain of methicillin-resistant *Staphylococcus* aureus with high-level β-lactam resistance contains mutations in three genes. *Antimicrob. Agents Chemother.* 54, 4900–4902 (2010).
- Dengler, V. et al. Mutation in the C-di-AMP cyclase dacA affects fitness and resistance of methicillin resistant Staphylococcus aureus. PLoS ONE 8, e73512 (2013).
- Rismondo, J. et al. Phenotypes associated with the essential diadenylate cyclase CdaA and its potential regulator CdaR in the human pathogen *Listeria monocytogenes*. *J. Bacteriol.* 198, 416–426 (2016).
- Whiteley, A. T. et al. c-di-AMP modulates *Listeria monocytogenes* central metabolism to regulate growth, antibiotic resistance and osmoregulation. *Mol. Microbiol.* 104, 212–233 (2017).
- Pham, H. T. et al. Cyclic di-AMP oversight of counter-ion osmolyte pools impacts intrinsic cefuroxime resistance in *Lactococcus lactis*. mBio 12, e00324-21 (2021).
- Nolan, A. C. et al. Purine nucleosides interfere with c-di-AMP levels and act as adjuvants to re-sensitize MRSA to β-lactam antibiotics. mBio 14, e02478-22 (2022).
- Galperin, M. Y. All DACs in a row: domain architectures of bacterial and archaeal diadenylate cyclases. J. Bacteriol. 205, e00023-23 (2023).
- 27. Popham, D. L. & Setlow, P. Phenotypes of *Bacillus subtilis* mutants lacking multiple class A high-molecular-weight penicillin-binding proteins. *J. Bacteriol.* **178**, 2079–2085 (1996).
- 28. Rosenberg, J. et al. Structural and biochemical analysis of the essential diadenylate cyclase CdaA from *Listeria monocytogenes*. *J. Biol. Chem.* **290**, 6596–6606 (2015).
- Cleverley, R. M. et al. The cell cycle regulator GpsB functions as cytosolic adaptor for multiple cell wall enzymes. *Nat. Commun.* 10, 261 (2019).
- Brunet, Y. R., Habib, C., Brogan, A. P., Artzi, L. & Rudner, D. Z. Intrinsically disordered protein regions are required for cell wall homeostasis in *Bacillus subtilis*. *Genes Dev.* 36, 970–984 (2022).
- van Heijenoort, J. Formation of the glycan chains in the synthesis of bacterial peptidoglycan. *Glycobiology* 11, 25R-36R (2001).
- Schwedt, I., Wang, M., Gibhardt, J. & Commichau, F. M. Cyclic di-AMP, a multifaceted regulator of central metabolism and osmolyte homeostasis in *Listeria monocytogenes*. microLife 4, uqad005 (2023).
- Zeden, M. S. et al. Cyclic di-adenosine monophosphate (c-di-AMP) is required for osmotic regulation in Staphylococcus aureus but dispensable for viability in anaerobic conditions. J. Biol. Chem. 293, 3180–3200 (2018).
- 34. Ye, M. et al. DhhP, a cyclic di-AMP phosphodiesterase of *Borrelia burgdorferi*, is essential for cell growth and virulence. *Infect. Immun.* **82**, 1840–1849 (2014).
- Yang, J. et al. Deletion of the cyclic di-AMP phosphodiesterase gene (cnpB) in Mycobacterium tuberculosis leads to reduced virulence in a mouse model of infection. Mol. Microbiol. 93, 65–79 (2014).
- 36. Bardetti, P., Barber, F. & Rojas, E. R. Non-linear stress-softening of the bacterial cell wall confers cell shape homeostasis. Preprint at bioRxiv https://doi.org/10.1101/2024.09.03.611099 (2024).

- 37. Rojas, E. R., Huang, K. C. & Theriot, J. A. Homeostatic cell growth is accomplished mechanically through membrane tension inhibition of cell-wall synthesis. *Cell Syst.* **5**, 578–590.e6 (2017).
- Brogan, A. P., Habib, C., Hobbs, S. J., Kranzusch, P. J. & Rudner, D. Z. Bacterial SEAL domains undergo autoproteolysis and function in regulated intramembrane proteolysis. *Proc. Natl Acad. Sci. USA* 120, e2310862120 (2023).
- 39. Midonet, C. et al. MacP bypass variants of *Streptococcus* pneumoniae PBP2a suggest a conserved mechanism for the activation of bifunctional cell wall synthases. *mBio* **14**, e02390-23 (2023).
- Yin, W. et al. A decade of research on the second messenger c-di-AMP. FEMS Microbiol. Rev. 44, 701–724 (2020).
- 41. Latoscha, A. et al. c-di-AMP hydrolysis by the phosphodiesterase AtaC promotes differentiation of multicellular bacteria. *Proc. Natl Acad. Sci. USA* **117**, 7392–7400 (2020).
- 42. Zhang, L., Li, W. & He, Z.-G. DarR, a TetR-like transcriptional factor, is a cyclic di-AMP-responsive repressor in *Mycobacterium* smegmatis. *J. Biol. Chem.* **288**, 3085–3096 (2013).
- Ba, X. et al. Truncation of GdpP mediates β-lactam resistance in clinical isolates of Staphylococcus aureus. J. Antimicrob. Chemother. 74, 1182–1191 (2019).
- Lai, L.-Y. et al. Altered PBP4 and GdpP functions synergistically mediate MRSA-like high-level, broad-spectrum β-lactam resistance in *Staphylococcus aureus*. mBio 15, e02889-23 (2024).
- 45. Chan, L. C. et al. Ceftobiprole- and Ceftaroline-resistant methicillin-resistant *Staphylococcus aureus*. *Antimicrob*. *Agents Chemother*. **59**, 2960–2963 (2015).
- Gostev, V. et al. In vitro ceftaroline resistance selection of methicillin-resistant Staphylococcus aureus involves different genetic pathways. Microb. Drug Resist. 25, 1401–1409 (2019).
- Sommer, A. et al. Mutations in the gdpP gene are a clinically relevant mechanism for β-lactam resistance in meticillin-resistant Staphylococcus aureus lacking mec determinants. Microb. Genom. 7, 000623 (2021).
- Deng, Y., Sun, M. & Shaevitz, J. W. Direct measurement of cell wall stress stiffening and turgor pressure in live bacterial cells. *Phys. Rev. Lett.* **107**, 158101 (2011).
- Gundlach, J. et al. An essential poison: synthesis and degradation of cyclic di-AMP in *Bacillus subtilis*. J. Bacteriol. 197, 3265–3274 (2015).
- 50. Bejerano-Sagie, M. et al. A checkpoint protein that scans the chromosome for damage at the start of sporulation in *Bacillus subtilis*. *Cell* **125**, 679–690 (2006).
- 51. Gibhardt, J. et al. An extracytoplasmic protein and a moonlighting enzyme modulate synthesis of c-di-AMP in *Listeria monocytogenes*. *Environ*. *Microbiol*. **22**, 2771–2791 (2020).
- Youngman, P. J., Perkins, J. B. & Losick, R. Genetic transposition and insertional mutagenesis in *Bacillus subtilis* with *Streptococcus* faecalis transposon Tn917. Proc. Natl Acad. Sci. USA 80, 2305–2309 (1983).
- 53. Harwood, C. R. & Cutting, S. M. Molecular Biological Methods for Bacillus (Wiley, 1990).
- 54. Gibson, D. G. et al. Enzymatic assembly of DNA molecules up to several hundred kilobases. *Nat. Methods* **6**, 343–345 (2009).
- 55. Wang, X., Brandão, H. B., Le, T. B. K., Laub, M. T. & Rudner, D. Z. Bacillus subtilis SMC complexes juxtapose chromosome arms as they travel from origin to terminus. Science **355**, 524–527 (2017).
- 56. Meeske, A. J. et al. MurJ and a novel lipid II flippase are required for cell wall biogenesis in *Bacillus subtilis*. *Proc. Natl Acad. Sci. USA* **112**, 6437–6442 (2015).
- 57. Patrick, J. E. & Kearns, D. B. MinJ (YvjD) is a topological determinant of cell division in *Bacillus subtilis*. *Mol. Microbiol*. **70**, 1166–1179 (2008).

- Rudner, D. Z., Fawcett, P. & Losick, R. A family of membrane-embedded metalloproteases involved in regulated proteolysis of membrane-associated transcription factors. *Proc. Natl Acad. Sci. USA* **96**, 14765–14770 (1999).
- 59. Miller, J. H. Experiments in Molecular Genetics (Cold Spring Harbor Laboratory, 1972).
- Wang, X. et al. Condensin promotes the juxtaposition of DNA flanking its loading site in *Bacillus subtilis*. Genes Dev. 29, 1661–1675 (2015).
- Fujita, M. & Sadaie, Y. Promoter selectivity of the *Bacillus subtilis* RNA polymerase 6k and CTH holoenzyme. *J. Biochem.* 124, 89–97 (1998).
- Haeusser, D. P., Schwartz, R. L., Smith, A. M., Oates, M. E. & Levin, P. A. EzrA prevents aberrant cell division by modulating assembly of the cytoskeletal protein FtsZ. *Mol. Microbiol.* 52, 801–814 (2004).
- 63. Ducret, A., Quardokus, E. M. & Brun, Y. V. MicrobeJ, a tool for high throughput bacterial cell detection and quantitative analysis. *Nat. Microbiol.* **1**, 16077 (2016).
- 64. Sievers, F. et al. Fast, scalable generation of high-quality protein multiple sequence alignments using Clustal Omega. *Mol. Syst. Biol.* **7**, 539 (2011).
- Sayers, E. W. et al. Database resources of the National Center For Biotechnology Information. *Nucleic Acids Res.* 50, D20–D26 (2021).
- Erdős, G., Pajkos, M. & Dosztányi, Z. IUPred3: prediction of protein disorder enhanced with unambiguous experimental annotation and visualization of evolutionary conservation. *Nucleic Acids Res.* 49, W297–W303 (2021).
- Letunic, I. & Bork, P. Interactive Tree Of Life (iTOL) v5: an online tool for phylogenetic tree display and annotation. *Nucleic Acids Res.* 49, W293–W296 (2021).
- Halladin, D. K. et al. Entropy-driven translocation of disordered proteins through the Gram-positive bacterial cell wall. Nat. Microbiol. 6, 1055–1065 (2021).

#### Acknowledgements

We thank A. Gründling and all members of the Bernhardt–Rudner supergroup for helpful advice, discussions and encouragement, and the MicRoN core for advice on fluorescence microscopy. Electron Microscopy Imaging and services were performed in the HMS Electron Microscopy Facility. Portions of this research were conducted on the O2 High Performance Computing Cluster, which is supported by

the Research Computing Group at Harvard Medical School. Support for this work was provided by National Institute of Health Grants R35GM145299, U19 A1158028 (D.Z.R.) and R35GM143057 (E.R.R.). A.P.B. was funded in part by NSF (DGE1745303) and NIH (F31AI181098).

#### **Author contributions**

A.P.B. and D.Z.R conceived the study. A.P.B. and P.B. performed the experiments and analyses. D.Z.R and E.R.R. supervised the study. A.P.B. and D.Z.R wrote the paper, with edits from P.B. and E.R.R.

#### **Competing interests**

The authors declare no competing interests.

#### **Additional information**

**Extended data** is available for this paper at https://doi.org/10.1038/s41564-025-02027-2.

**Supplementary information** The online version contains supplementary material available at https://doi.org/10.1038/s41564-025-02027-2.

**Correspondence and requests for materials** should be addressed to David Z. Rudner.

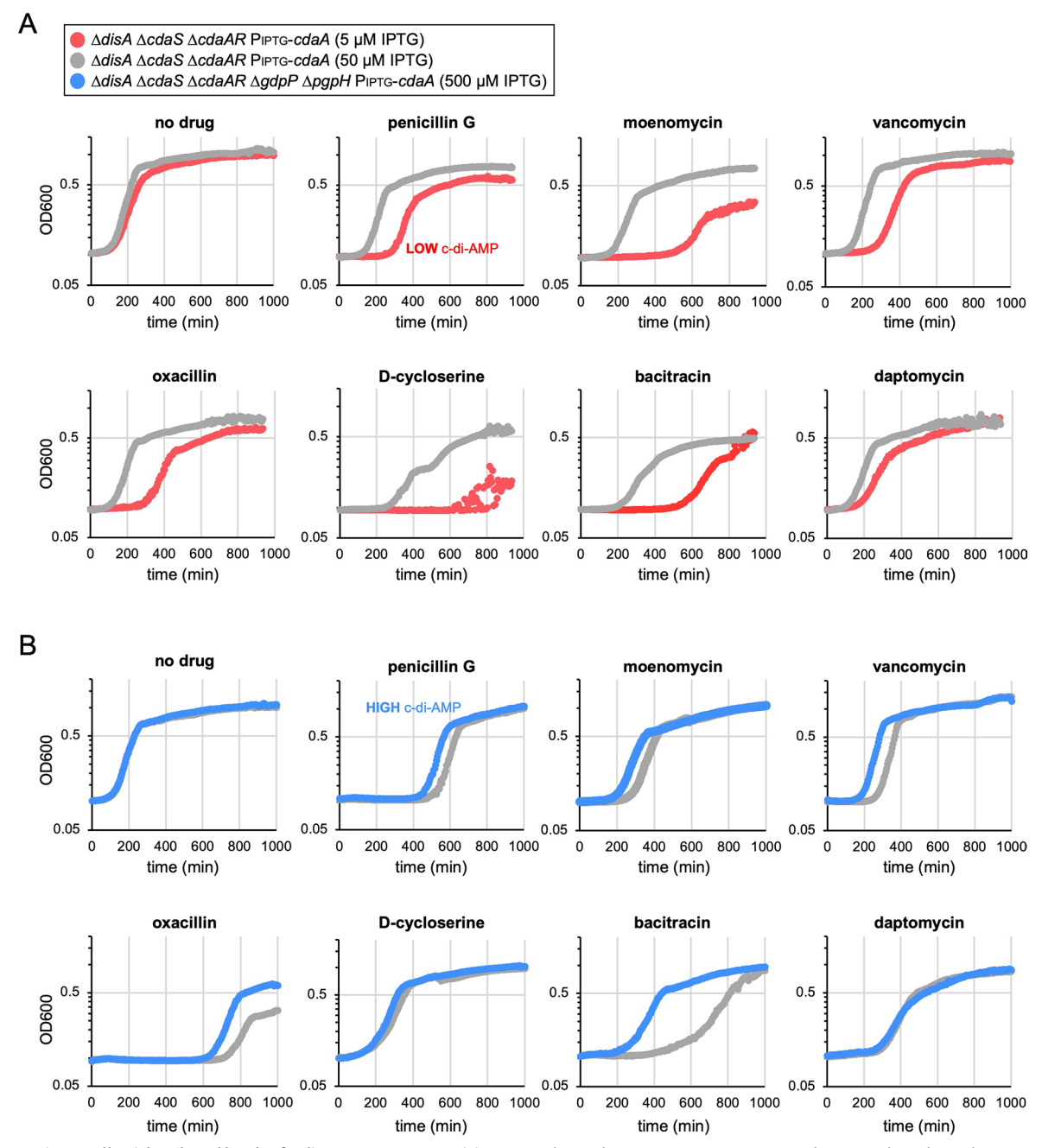
**Peer review information** *Nature Microbiology* thanks Fabian Commichau, Daniel Kearns and the other, anonymous, reviewer(s) for their contribution to the peer review of this work.

**Reprints and permissions information** is available at www.nature.com/reprints.

**Publisher's note** Springer Nature remains neutral with regard to jurisdictional claims in published maps and institutional affiliations.

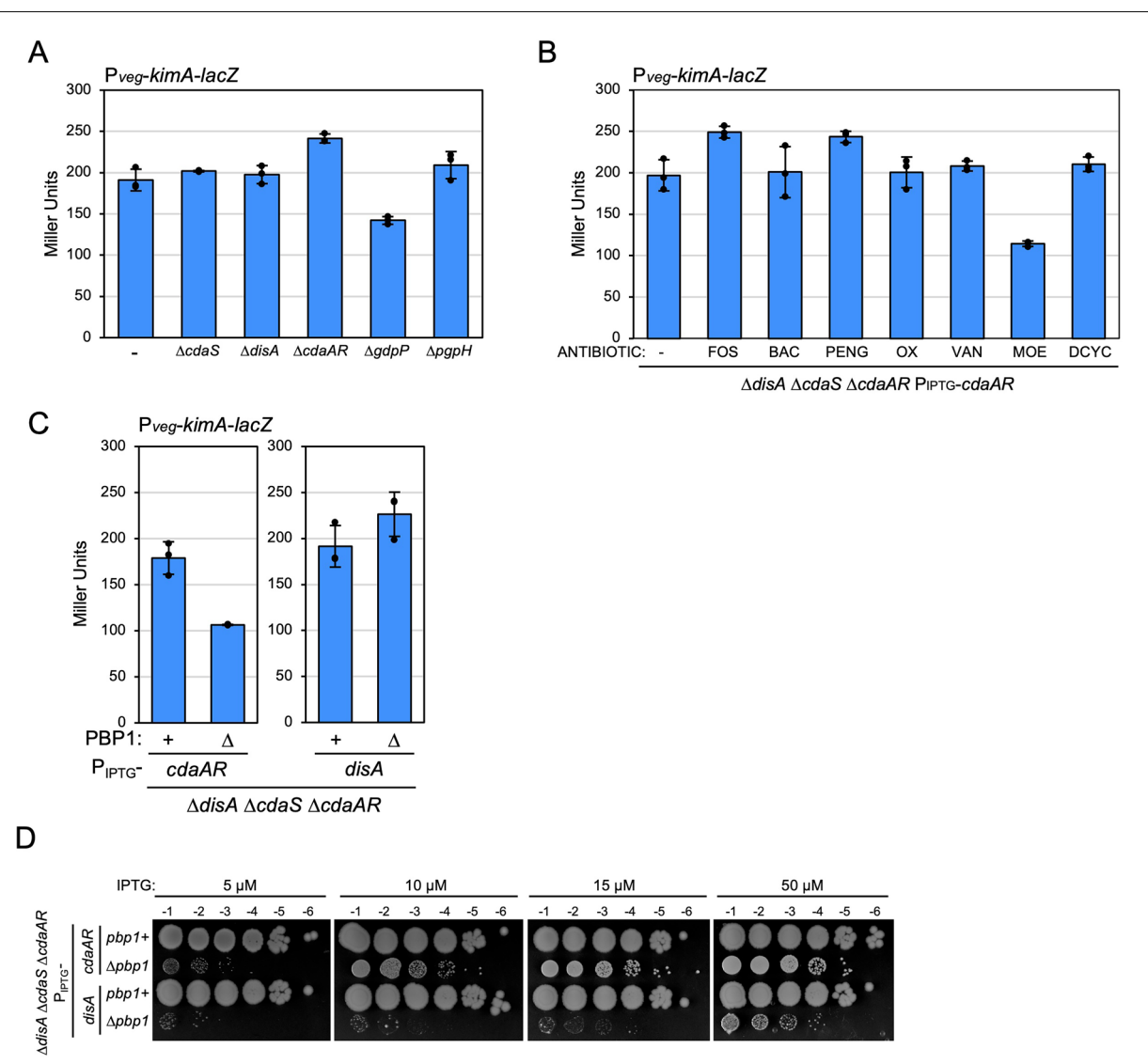
Springer Nature or its licensor (e.g. a society or other partner) holds exclusive rights to this article under a publishing agreement with the author(s) or other rightsholder(s); author self-archiving of the accepted manuscript version of this article is solely governed by the terms of such publishing agreement and applicable law.

© The Author(s), under exclusive licence to Springer Nature Limited 2025



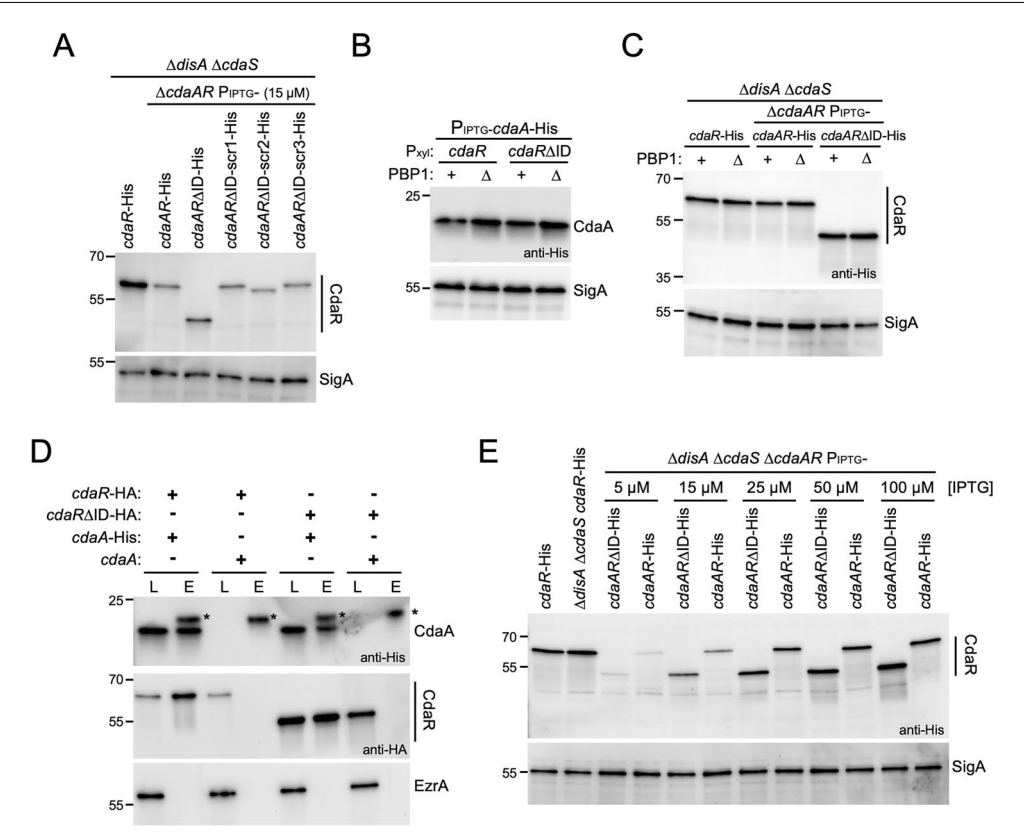
Extended Data Fig. 1 | Cells with reduced levels of c-di-AMP are more sensitive to envelope-targeting antibiotics, while cells with increased levels of c-di-AMP are more resistant. Representative growth curves of the indicated strains grown in LB with 5,50  $\mu$ M, or 500  $\mu$ M IPTG treated with sub-inhibitory concentrations of the indicated antibiotics. (A) Red lines show cells that express low levels of CdaA with 5  $\mu$ M IPTG and grey lines show cells that express wild-type levels of

CdaA with 50  $\mu$ M IPTG. 50  $\mu$ M IPTG is closest to physiological expression levels (Extended Data Fig. 3e). (B) Blue lines show cells that express high levels of CdaA with 500  $\mu$ M IPTG in the absence of the phosphodiesterases GdpP and PgpH. All experiments in this figure were performed in biological triplicate and representative growth curves are shown.



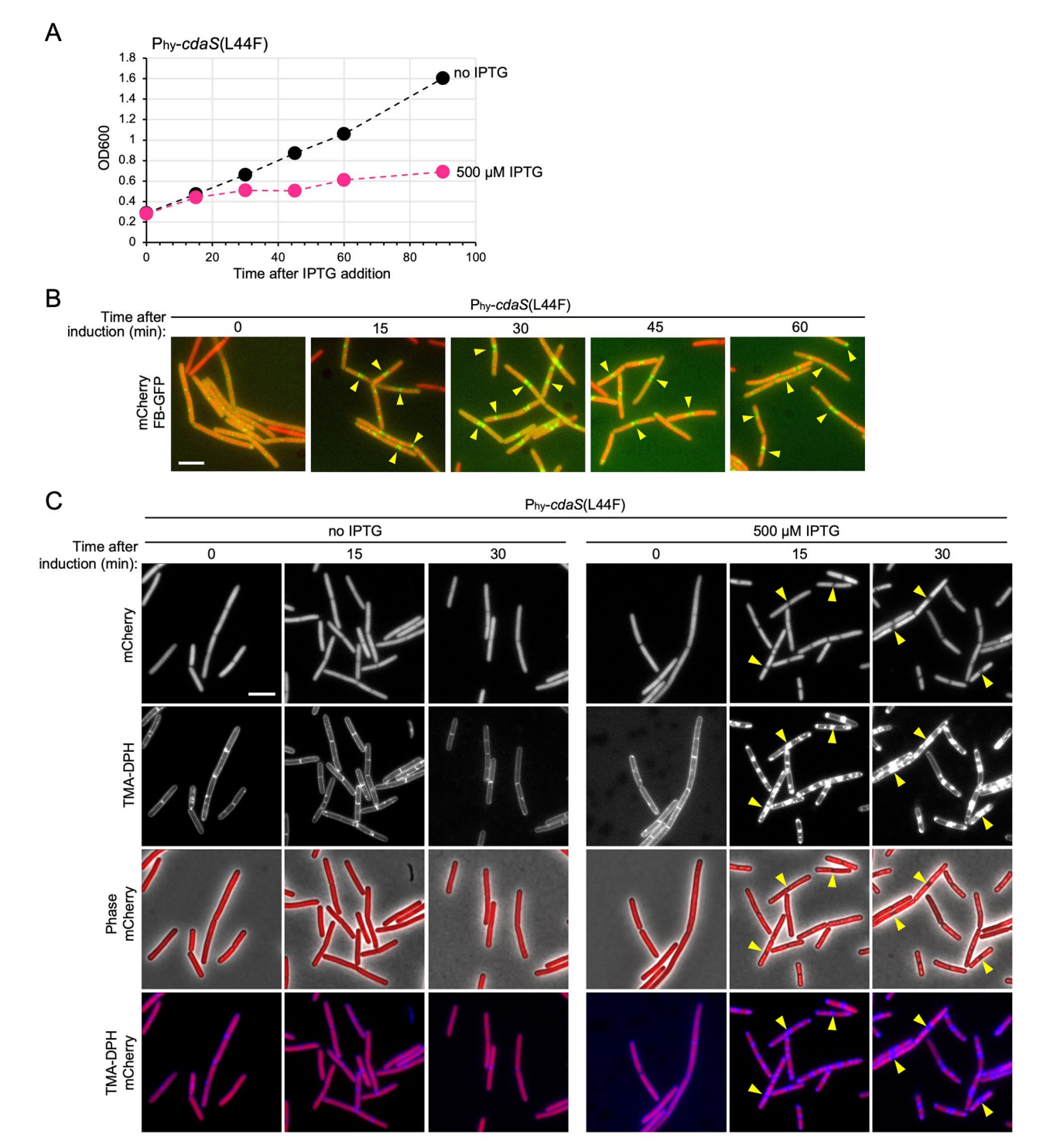
Extended Data Fig. 2 | Analysis of growth and c-di-AMP levels in mutants and after antibiotic exposure. (A) Bar graph showing  $\beta$ -galactosidase activity from the riboswitch reporter of the indicated *B. subtilis* deletion mutants. Cells lacking *cdaAR* have lower c-di-AMP and cells lacking *gdpP* have higher c-di-AMP. All measurements were performed in biological triplicate except the  $\Delta cdaS$  condition which was performed in duplicate. (B) Bar graph showing  $\beta$ -galactosidase activity from the *kimA* reporter in cells lacking *disA*, *cdaS*, and *cdaAR*, and harbouring an IPTG-regulated allele of *cdaAR* in the presence of 50  $\mu$ M IPTG. The strain was treated with sub-inhibitory concentrations (0.5X MIC) of fosfomycin (FOS), bacitracin (BAC), penicillin G (PENG), oxacillin

(OX), vancomycin (VAN), moenomycin (MOE), D-cycloserine (DCYC). Cells only increase c-di-AMP levels in the presence of moenomycin that inhibits the glycosyltransferase activity of class A PBPs. (C) Bar graph showing  $\beta$ -galactosidase activity from the kimA riboswitch reporter in cells expressing CdaAR or DisA as the only c-di-AMP cyclase in the presence of absence of PBP1. The center of error represents the average, and the error bars represent the standard deviation across three biological replicates. (D) 10-fold serial dilutions of the indicated strains spotted on LB agar supplemented with the indicated IPTG concentrations. CdaAR is critical in the absence of PBP1.



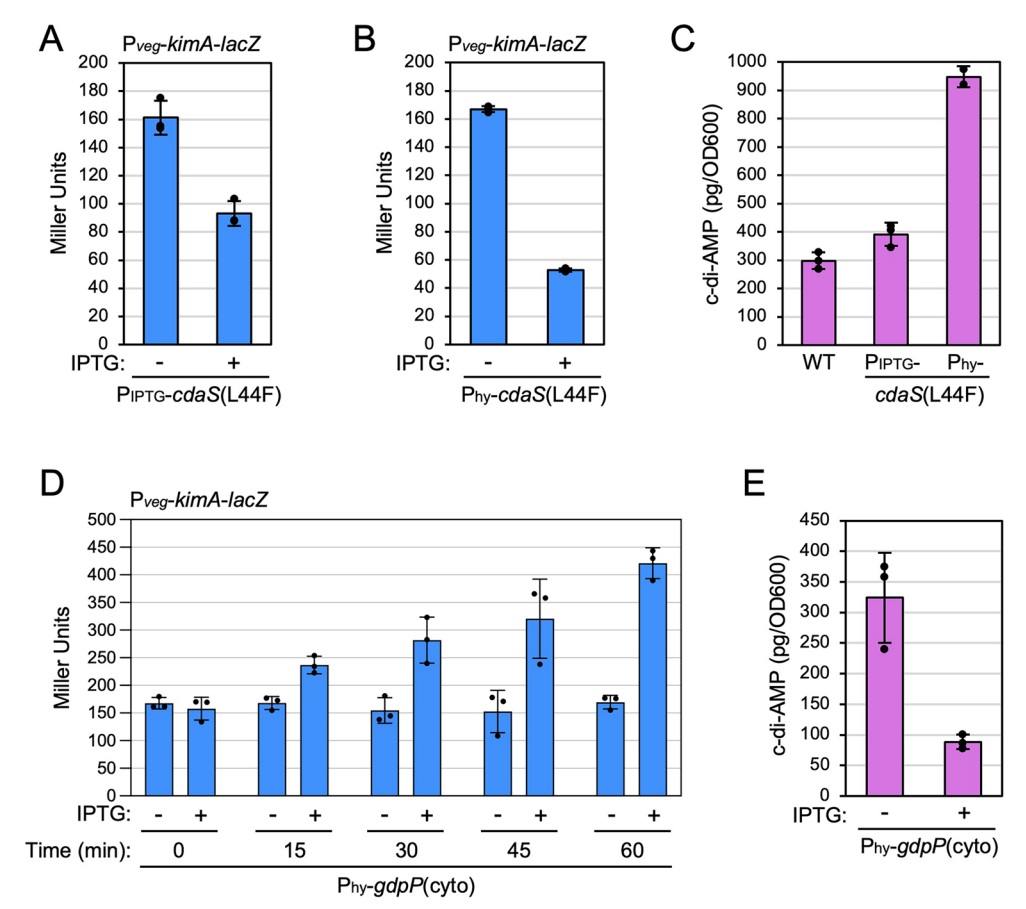
**Extended Data Fig. 3** | **Analysis of CdaA and CdaR variants.** (**A**) Immunoblot of *B. subtilis* cells expressing *cdaR*-His at its native locus (first lane) or *cdaR*-His and variants at an ectopic location under IPTG-control with 15  $\mu$ M IPTG. All strains lack *disA* and *cdaS*. (**B**) Immunoblot of cells expressing CdaA-His under IPTG-inducible control with 500  $\mu$ M IPTG and CdaR-HA or CdaR $\Delta$ ID-HA under xylose-inducible control with 30 mM xylose. *cdaA* and *cdaR* were inserted at separate genomic location. The strains express (+) or lack ( $\Delta$ ) PBP1. (**C**) Cells expressing CdaR-His at its native locus (lanes 1 & 2) compared to CdaA-CdaR-His with and without its IDR ( $\Delta$ ID) under IPTG-inducible control at an ectopic locus with 50  $\mu$ M IPTG. (**D**) Immunoblots from a co-immunoprecipitation assay using anti-His resin and detergent-solubilized membrane fractions. The load (L) and eluate (E) were probed for CdaA-His, CdaR-HA, CdaR $\Delta$ ID-HA and the membrane protein

EzrA. The *B. subtilis* strains expressed CdaA with or without a His-tag under IPTG-inducible control with 500  $\mu$ M IPTG and CdaR-HA with or without its IDR under xylose-inducible control with 30 mM xylose. A non-specific cross-reactive band is indicated (\*). The CdaA:CdaR complex does not require CdaR's IDR. The co-IP was performed in biological duplicate and a representative experiment is shown. (**E**) Immunoblot of *B. subtilis* cells expressing CdaR-His at its native locus (lanes 1&2) or CdaA-CdaR-His with and without its IDR under IPTG-inducible control expressed with the indicated IPTG concentrations. SigA was used to control for loading in panels (**A**), (**B**), (**C**), and (**E**). 50  $\mu$ M IPTG is closest to physiological expression of CdaA and CdaR. All Immunoblots are representative of three biological replicates.



**Extended Data Fig. 4** | **An acute increase in c-di-AMP causes membrane invaginations.** (**A**) Growth curve of cells containing Phy-cdaS(L44F) induced with 500  $\mu$ M (pink) or without (black) IPTG. (**B**) Representative fluorescence images of cells grown in the presence of 500  $\mu$ M IPTG for the indicated times. Cells were harvested at the indicated times, but images were acquired -5 minutes later due to cell concentration, mounting, and imaging. Cells contain constitutively

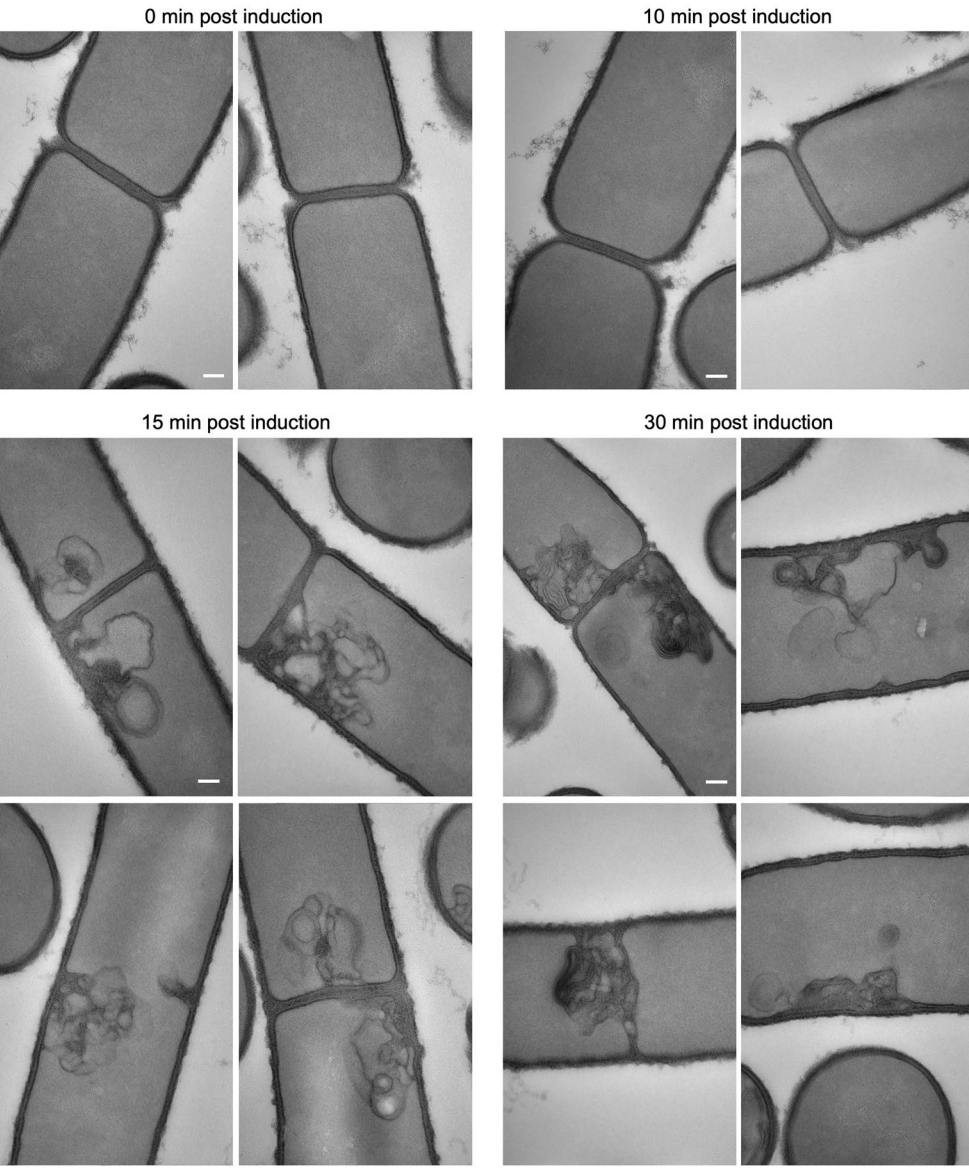
expressed cytoplasmic mCherry and membranes are labeled using the membrane protein SpoIVFB-GFP (FB-GFP). Sites of cytoplasmic retraction and membrane invagination are highlighted (yellow carets). (C) The same experiment as described in (B) with membranes stained with the membrane dye TMA-DPH. Scale bars indicate 5  $\mu m$ .



Extended Data Fig. 5 | Analysis of c-di-AMP levels in cells expressing cdaS(L44F) or gdpP(cyto). (A, B) Bar graphs showing  $\beta$ -galactosidase activity from the kimA riboswitch reporter in B. subtilis strains expressing cdaS(L44F) from (A) the Pspank (PIPTG) or (B) the Phyperspank (Phy) promoters. Expression was induced with 500  $\mu$ M IPTG for 90 minutes. (C) Bar graph showing c-di-AMP levels as measured by ELISA assay in the same conditions as shown in (A, B). Values were normalized to the culture OD<sub>600</sub>. All ELISA measurements were

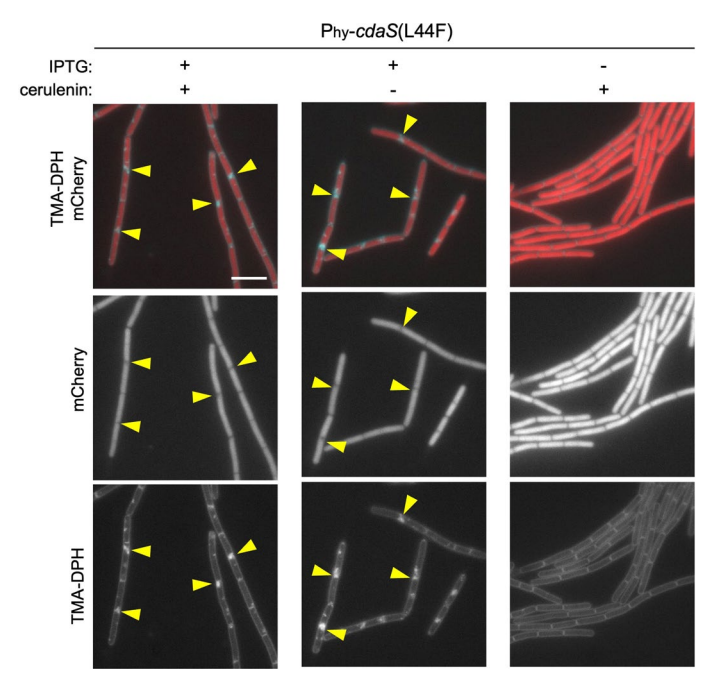
performed in biological triplicate except the  $P_{\rm hy}$  condition which was performed in duplicate. (**D**) Bar graph showing  $\beta$ -galactosidase activity from the kimA reporter of cells expressing Phy- $gdpP({\rm cyto})$ . Samples were taken at the indicated timepoints after addition (+) of 500  $\mu$ M IPTG. (**E**) Bar graph showing c-di-AMP levels normalized to  $OD_{600}$  as measured by ELISA after 45 minutes of induction with Phy- $gdpP({\rm cyto})$ . In all panels, the center of error represents the average, and the error bars represent the standard deviation across three biological replicates.

#### Phy-cdaS(L44F)



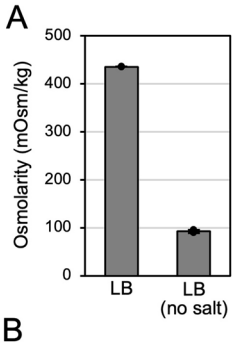
 $\label{lem:continuous} \textbf{Extended Data Fig. 6} \ | \ An acute increase in c-di-AMP causes membrane invaginations. Transmission electron micrographs of exponentially growing cells harboring Phy-cdaS(L44F) before and at indicated timepoints after the$ 

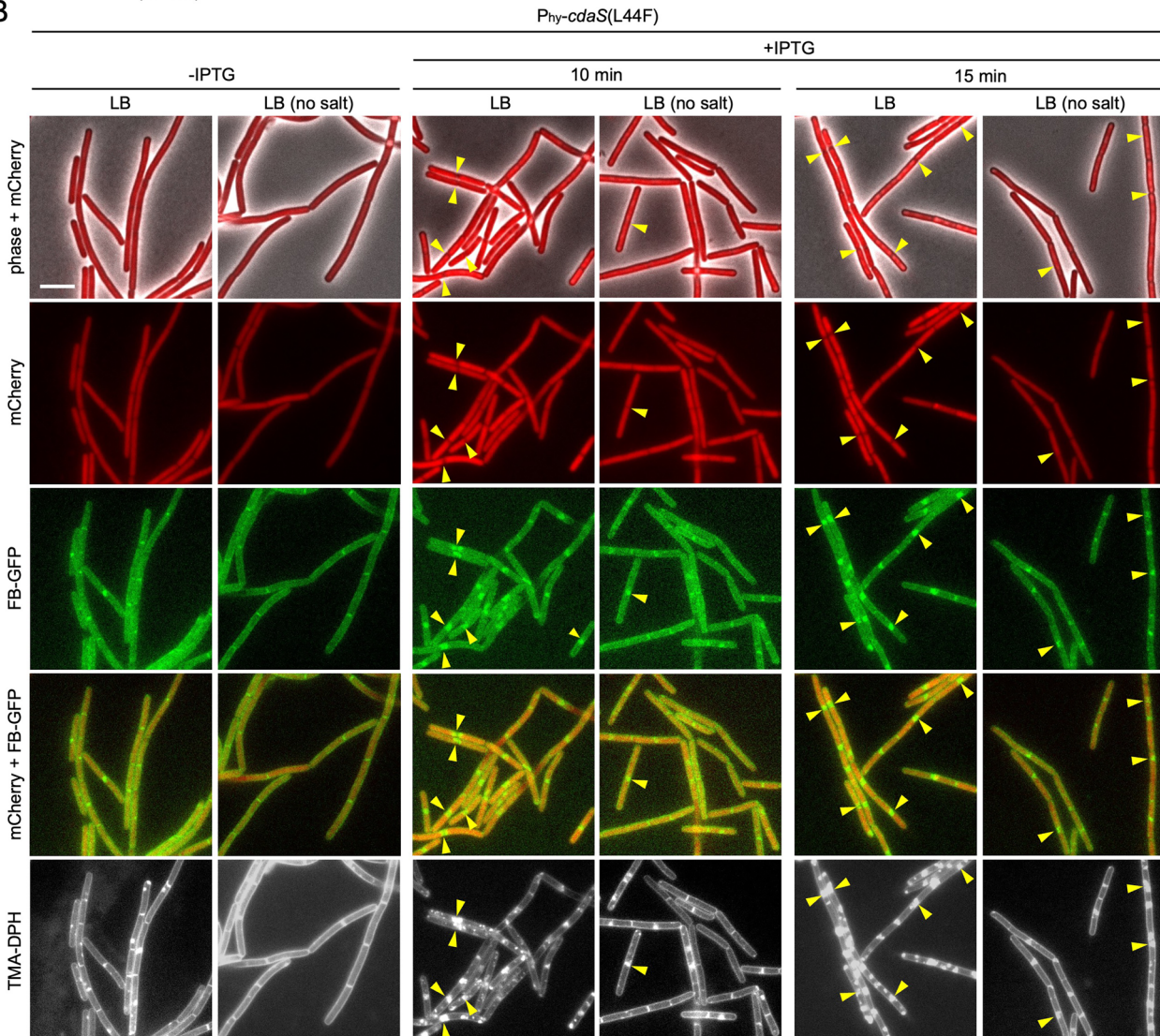
addition of 500  $\mu M$  IPTG. Cells were immediately fixed after harvest. Scale bars indicate 100 nm. Sample preparation and imaging were performed in biological duplicate and representative images are shown.



Extended Data Fig. 7 | An acute increase in c-di-AMP levels causes membrane invaginations independent of phospholipid biosynthesis. Representative images of B. Subtilis cells harboring Phy-CdaS(L44F). Cells were induced with 500  $\mu$ M IPTG for 10 min and then treated with cerulenin (12.5  $\mu$ g/mL) to block phospholipid synthesis for 5 min prior to harvest. Images were acquired -5 minutes later due to cell concentration, mounting, and imaging. The delay in cerulenin addition (10 min after IPTG-induction) was chosen based on control experiments showing that the drug rapidly inhibits transcription from an IPTG-regulated promoter (Supplementary Fig. 6). Importantly, no membrane invaginations are detectable at 10 min after IPTG addition (Extended

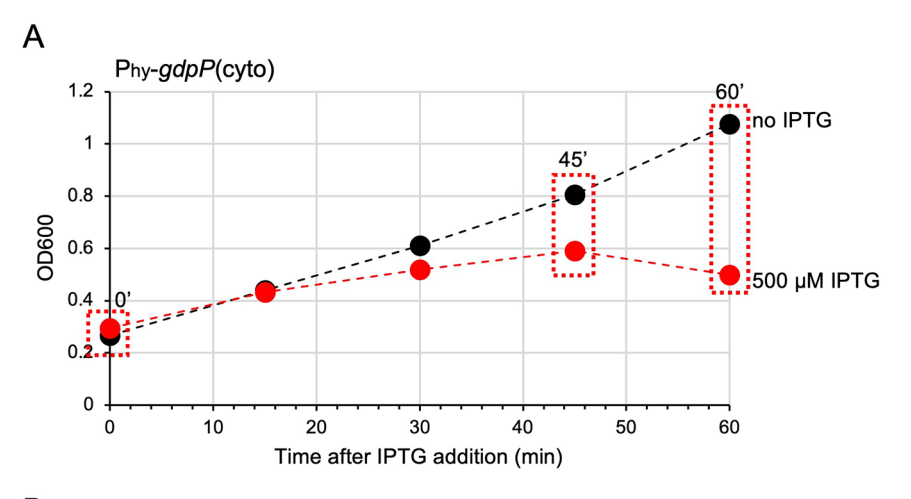
Data Fig. 6). Thus, cerulenin treatment at 10 minutes enabled cdaS(L44F) expression and inhibition of phospholipid biosynthesis prior to the generation of membrane invaginations. Membrane accumulation did not increase over the next 75 minutes in cerulenin treated cells, suggesting that the severity of the membrane invaginations is partially due to uncoupled phospholipid synthesis from growth. Cells constitutively expressed cytoplasmic mCherry and were stained with TMA-DPH to label membranes. Sites of membrane invagination in the presence or absence of cerulenin are highlighted (yellow carets). Scale bar indicates  $5~\mu m$ .

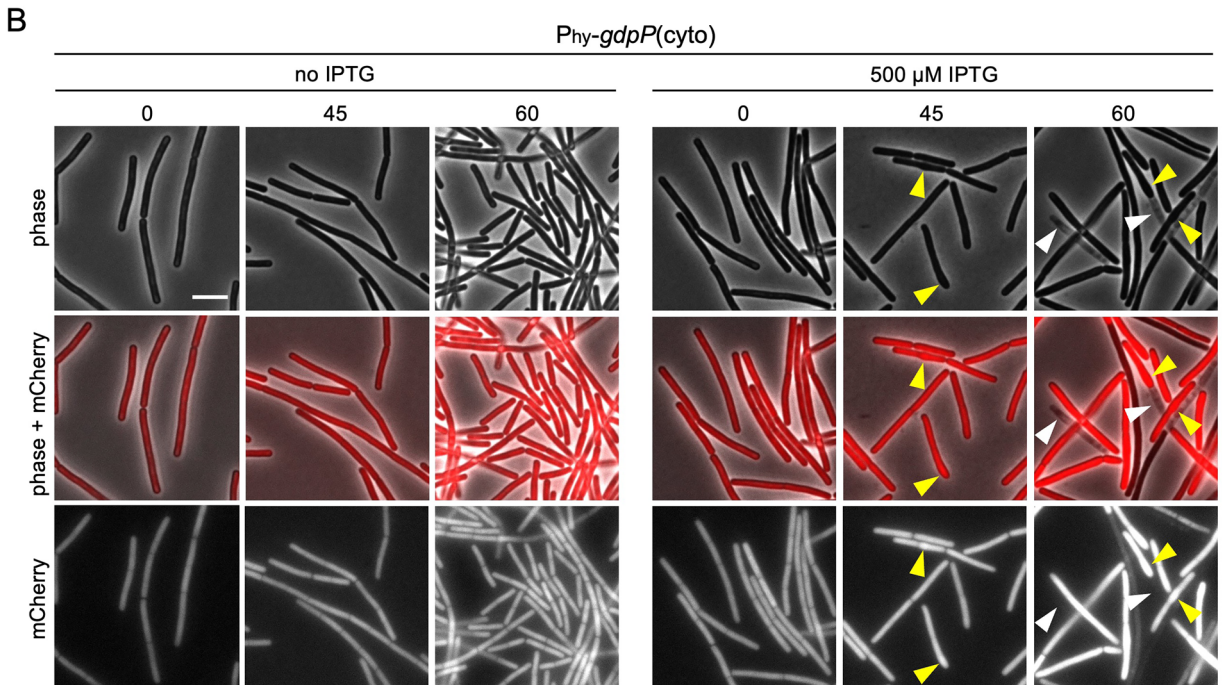




Extended Data Fig. 8 | Membrane invaginations caused by an acute increase in c-di-AMP depend on the external osmolarity. (A) Bar graph showing the osmolarity of LB and LB lacking salt (no salt) as measured using an osmometer. The center of error represents the average and error bars indicate the standard deviation among three replicates. (B) Representative fluorescence micrographs of cells harboring Phy-cdaS(L44F) before (-IPTG) or at indicated time points after the addition of 500  $\mu$ M IPTG (+ IPTG). 10 or 15 min after induction, cells

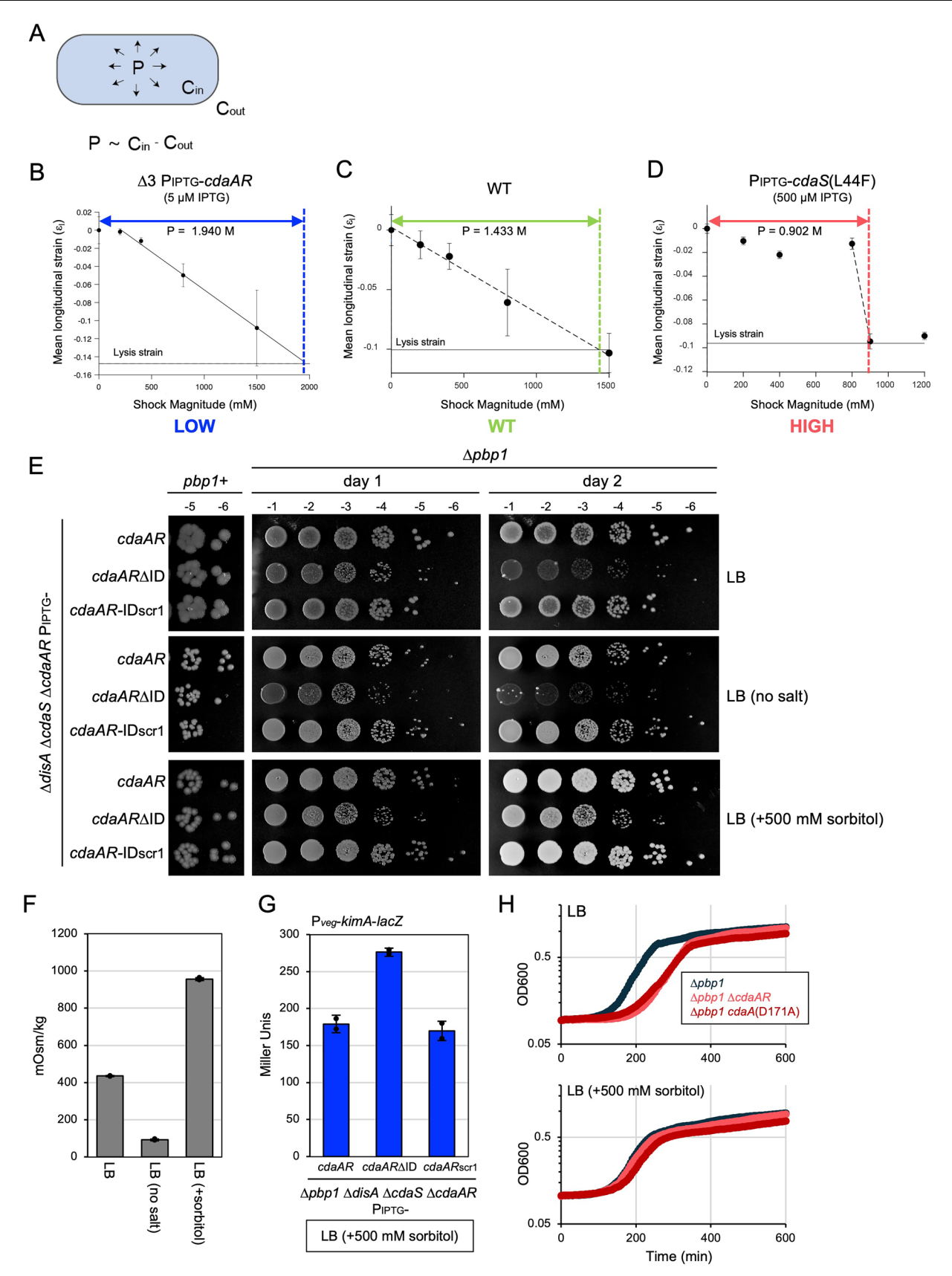
were pelleted, resuspended in LB or LB (no salt), spotted onto LB or LB (no salt) 2% agarose pads and imaged 5 min after harvest. Cells contain constitutively expressed cytoplasmic mCherry and membranes were labeled using a constitutively expressed membrane protein SpolVFB-GFP (FB-GFP) and the membrane dye TMA-DPH. Carets highlight sites of cytoplasmic retraction and membrane invagination. Low external osmolarity (LB no salt) largely suppresses the membrane invagination caused by high c-di-AMP. Scale bars indicate 5  $\mu m$ .





Extended Data Fig. 9 | An acute decrease in c-di-AMP causes bulging and lysis. (A) Growth curves of *B. subtilis* cells harboring Phy-gdpP(cyto) that lacks its transmembrane and PAS domains induced with 500  $\mu$ M IPTG (red line) or without inducer (black line). (B) Representative fluorescence and phase-contrast images of Phy-gdpP(cyto) cells at the indicated time points in the presence or absence

of 500  $\mu$ M IPTG. Cells were harvested at the indicated timepoints, and images were acquired -5 minutes after harvest due to cell concentrating, mounting, and imaging. Cells constitutively express cytoplasmic mCherry. Sites of cell bulging (yellow carets) and lysis (white carets) are indicated. Scale bar indicates 5  $\mu$ m.



 $\textbf{Extended Data Fig. 10} \, | \, \textbf{See next page for caption.}$ 

Extended Data Fig. 10 | Cyclic-di-AMP controls cellular turgor. (A) Diagram of a cell inflated by turgor pressure  $P = RT(C_{in}-C_{out})$ , where  $C_{in}$  is the cytosolic osmolarity and  $C_{out}$  is the extracellular osmolarity. Adapted from *Bardetti* et al<sup>36</sup>. (B,C,D) Osmotic force extension curves and lysis strains of cells lacking disA, cdaS, cdaAR and harboring PIPTG-cdaAR grown with 5 μM IPTG (**B**), wild-type (WT) (C), and cells with PIPTG-cdaS(L44F) grown with 500 μM IPTG (D). Cells grown in LB in a microfluidic chamber were exposed to a hyperosmotic shock of LB containing the indicated molarity of sorbitol (x-axis), and the mean percent change in cell length  $(\varepsilon_l)$  in response to the shock [(length<sub>final</sub>-length<sub>initial</sub>)/  $length_{final}$ ] was measured. The solid horizontal line indicates the average change in cell length (Lysis strain) upon lysis with detergent. Lysis strain was determined by growing cells in LB in a microfluidic chamber and measuring the percent  $change\ in\ cell\ length\ [(length_{final}\text{-}length_{initial}/length_{final}]\ before\ and\ after\ exposure$ to LB containing 5% of the anionic detergent N-lauroylsarcosine. Dotted lines represent the linear regression used to find pressure, which was calculated as the shock magnitude that causes contraction of length to the rest length upon cell lysis. The colored dotted lines indicate the pressure (P) in units of molarity shown in Fig. 5k. For the lysis experiments, n = 136,82,116 for LOW, WT, and HIGH, respectively. For the hyperosmotic shock experiments, the n for increasing

sorbitol concentration was n = 104,104,104,68(LOW), n = 116,116,116,376(WT), and n = 50,50,50,59,74 (HIGH). Error bars indicate average longitudinal strain and standard error among replicates. (E) Spot dilutions on LB, LB (no salt), or LB (+500 mM sorbitol) agar all containing 15 µM IPTG. Strains lack disA, cdaS, and cdaAR and harbour the indicated IPTG-regulated allele of cdaAR. Images are shown after one and two days of incubation. High osmolarity suppresses the growth defects associated with  $cdaAR-\Delta ID$  expression in the absence of PBP1. (F) Bar graph showing the osmolarities of the indicated media as measured by an osmometer. The center of error represents the average and error bars represent the standard deviation among three replicates. (G) Bar graph showing  $\beta$ -galactosidase activity from the kimA riboswitch reporter of strains assayed in (A) grown to mid-log in LB ( + 500 mM sorbitol). The strains lack pbp1, disA, cdaS, and cdaAR and express the indicated cdaAR allele with 50 µM IPTG. High external osmolarity does not impact the intracellular c-di-AMP levels of the strains. The center of error represents the average and error bars indicate the standard deviation between two biological replicates. (H) Growth curves of the indicated strains in LB and LB (  $\pm$  500 mM sorbitol). High osmolarity suppresses the growth defect associated with cdaA mutants. Spot titers and growth curves are representative of three biological replicates.

## nature portfolio

Corresponding author(s):	David Rudner
Last updated by author(s):	Apr 16, 2025

## Reporting Summary

Nature Portfolio wishes to improve the reproducibility of the work that we publish. This form provides structure for consistency and transparency in reporting. For further information on Nature Portfolio policies, see our <u>Editorial Policies</u> and the <u>Editorial Policy Checklist</u>.

_				
C.	tっ	+1	ct	ics
. )			21	11.

For	all statistical analyses, confirm that the following items are present in the figure legend, table legend, main text, or Methods section.
n/a	Confirmed
	The exact sample size (n) for each experimental group/condition, given as a discrete number and unit of measurement
	A statement on whether measurements were taken from distinct samples or whether the same sample was measured repeatedly
	The statistical test(s) used AND whether they are one- or two-sided  Only common tests should be described solely by name; describe more complex techniques in the Methods section.
$\boxtimes$	A description of all covariates tested
$\boxtimes$	A description of any assumptions or corrections, such as tests of normality and adjustment for multiple comparisons
	A full description of the statistical parameters including central tendency (e.g. means) or other basic estimates (e.g. regression coefficient) AND variation (e.g. standard deviation) or associated estimates of uncertainty (e.g. confidence intervals)
	For null hypothesis testing, the test statistic (e.g. <i>F</i> , <i>t</i> , <i>r</i> ) with confidence intervals, effect sizes, degrees of freedom and <i>P</i> value noted <i>Give P values as exact values whenever suitable.</i>
$\boxtimes$	For Bayesian analysis, information on the choice of priors and Markov chain Monte Carlo settings
$\boxtimes$	For hierarchical and complex designs, identification of the appropriate level for tests and full reporting of outcomes
$\boxtimes$	Estimates of effect sizes (e.g. Cohen's <i>d</i> , Pearson's <i>r</i> ), indicating how they were calculated
	Our web collection on statistics for biologists contains articles on many of the points above.

#### Software and code

Policy information about availability of computer code

Data collection Microscopy data collection was performed using Nikon Elements 4.3 software.

Data analysis

which oscopy data collection was performed daing mixon Elements 4.5 software.

Microscopy data analysis was performed using ImageJ (version 2.9) software.

All graphs were generated in GraphPad Prism 10 or Microsoft Excel Version 16.89.1

Homology searches were performed using psi-blast version 2.2.1 (https://blast.ncbi.nlm.nih.gov/Blast.cgi)

Multiple sequence alignments were generated using the publicly available software Clustal Omega version 1.2.2

Superplotter plots were generated using https://superviolin.streamlit.app/ (published 2021)

Phylogenetic trees were constructed using iTOL version 7.1 (https://itol.embl.de/)

Spot titer contrast was set using Photoshop version 24.3.0

Cell size quantification was performed using MicrobeJ version 5.13I (https://www.microbej.com/)

For manuscripts utilizing custom algorithms or software that are central to the research but not yet described in published literature, software must be made available to editors and reviewers. We strongly encourage code deposition in a community repository (e.g. GitHub). See the Nature Portfolio guidelines for submitting code & software for further information.

#### Data

Policy information about availability of data

All manuscripts must include a data availability statement. This statement should provide the following information, where applicable:

- Accession codes, unique identifiers, or web links for publicly available datasets
- A description of any restrictions on data availability
- For clinical datasets or third party data, please ensure that the statement adheres to our policy

No large-scale datasets were generated over the course of this study. All relevant data is available in the supplementary material. Raw data for all graphs has been uploaded as source data. Uncropped immunoblots are included in the supplementary information. Primers, synthetic DNA constructs and strains used can be found in supplementary tables. The RefSeq database downloaded from NCBI (https://ftp.ncbi.nih.gov/refseq/release/) as of June, 2019 was used for the described bioinformatics analysis. The phylogenetic tree was generated from 5767 unique bacterial taxa assembled from the assembled reference genomes in the prokaryotic RefSeg database as of June, 2019.

#### Research involving human participants, their data, or biological material

Policy information about studies v	vith <u>numan participants or numan data</u> . See also policy information about <u>sex, gender (identity/presentation),</u>
and sexual orientation and race, e	thnicity and racism.
Reporting on sev and gender	N/A

Reporting on sex and gender	N/A
Reporting on race, ethnicity, or other socially relevant groupings	N/A
Population characteristics	N/A
Recruitment	N/A

Note that full information on the approval of the study protocol must also be provided in the manuscript.

## Field-specific reporting

lease select the one below that is the best fit for your research. If you are not sure, read the appropriate sections before making your selection.
---

Behavioural & social sciences For a reference copy of the document with all sections, see <u>nature.com/documents/nr-reporting-summary-flat.pdf</u>

## Life sciences study design

All studies must disclose on these points even when the disclosure is negative.

N/A

Sample size

X Life sciences

Ethics oversight

For microscopy experiments, no sample size calculations were calculated. All analyses were performed on an arbitrarily large number of cells that was representative of the population. At least ten images from areas around each pad were taken. As the cells were always homogeneous throughout the frame(s) and all frames contained around 50-500 cells, sample size calculations were unnecessary. All cell size quantification was performed on >70 cells in three biological replicates. Quantification of PI-brightness was performed on >1000 cells per condition. Il other experiments involve bulk assays using greater than 10^7 cells and were performed in at least triplicate.

Ecological, evolutionary & environmental sciences

Data exclusions

No data excluded.

Replication

All experiments were carried out in biological triplicate unless otherwise indicated with the exception of TEM images which were carried out in biological duplicate. Figure legends and the methods spell out replicates for each experiment described. For microscopy experiments, at least 10 fields of view were analyzed.

Randomization

We did not randomize samples, as after experimental setup, all measurements and analysis were performed identically across all conditions.

Blinding

We did not blind samples, as after experimental setup, all measurements and analysis were performed identically across all conditions.

## Reporting for specific materials, systems and methods

We require information from authors about some types of materials, experimental systems and methods used in many studies. Here, indicate whether each material, system or method listed is relevant to your study. If you are not sure if a list item applies to your research, read the appropriate section before selecting a response.

τ	3
٠	3
	\
	ċ
	Ç
	ũ

Materials & experime	ental systems	Methods
n/a Involved in the study	,	n/a Involved in the study
Antibodies		ChIP-seq
Eukaryotic cell lines	S	Flow cytometry
Palaeontology and	archaeology	MRI-based neuroimaging
Animals and other	organisms	
Clinical data		
Dual use research of	of concern	
Antibodies		
Antibodies used	1) THE™ His Tag Antibody (us	sed at 1:4000), mAb, Mouse, Genscript, Cat A00186, Clone 6G2A9.
	2) anti-SigA (used at 1:10000	), polyclonal, Gift of Masaya Fujita (University of Houston).
		L)-HRP Conjugate #1706516 (Used at 1:20000), BioRad.
		L)-HRP Conjugate #1706515 (Used at 1:3000), BioRad.
		mAb, Sigma, Cat H9658, Clone HA-7.
	6) anti-EzrA (used at 1:10000	)) , polyclonal, Gift of Petra Levin (WashU St. Louis).
available at: https://www.genscript.com/anti The anti-HA antibody is commercially availab		en used numerous times in other publications and validation is available on the company website, nscript.com/antibody/A00186-THE_His_Tag_Antibody_mAb_Mouse.html
		mercially available from Sigma and validation is available on their website (https://
		en/product/sigma/h9658?srsltid=AfmBOoo2lyO-
	0_ 0_ ,	wHnu6EkrSPxsZ-8TRNPO6ye) It has been used in numerous other publications.
		enerated by Masaya Fujita and has been used in numerous publications as a loading control for B.
	0 0	from our lab and others. Specificity of anti-SigA antibodies were confirmed with purified SigA protein
	and using lysates from B sub	utilis cell expressing different levels of SigA under IPTG control

membrane proteins. Specificity of anti-EzrA antibodies was confirmed using a B. subtilis ∆ezrA mutant.

#### **Plants**

Seed stocks

Report on the source of all seed stocks or other plant material used. If applicable, state the seed stock centre and catalogue number. If plant specimens were collected from the field, describe the collection location, date and sampling procedures.

The anti-EzrA antibody was generated by Petra Levin and has been used in numerous publications as a loading control for B. subtilis

Novel plant genotypes

Describe the methods by which all novel plant genotypes were produced. This includes those generated by transgenic approaches, gene editing, chemical/radiation-based mutagenesis and hybridization. For transgenic lines, describe the transformation method, the number of independent lines analyzed and the generation upon which experiments were performed. For gene-edited lines, describe the editor used, the endogenous sequence targeted for editing, the targeting guide RNA sequence (if applicable) and how the editor

Authentication

was applied.

Describe any authentication procedures for each seed stock used or novel genotype generated. Describe any experiments used to assess the effect of a mutation and, where applicable, how potential secondary effects (e.g. second site T-DNA insertions, mosiacism, off-target gene editing) were examined.